A Special Core Analyses Study Of Selected Samples From The Well : Casino - 2

Australia

Prepared for
SANTOS LIMITED

APRIL 2003

File: PRP-02059

Rock Properties Group
Core Laboratories Australia Pty. Ltd.
Perth
Australia

24th April 2003

Santos Limited
Santos House
91 King William Street
ADELAIDE, SA 5000

Attention : Andy Pietsch

Subject : Special Core Analysis
Well : Casino - 2
File : PRP-02059

Dear Andy,

Presented herein is the final report of the Special Core Analyses conducted on the selected core plug samples from the Well : Casino – 2.

Thank you for the opportunity to have been of service to Santos Limited. If you have any questions regarding these results or if we can be of any further assistance please do not hesitate to contact us.

Yours sincerely,
CORE LABORATORIES

Ajit Singh
Supervisor - Rock Properties Group Perth

CONTENTS

SECTION 1
SUMMARY & INTRODUCTION

Summary of Results

Routine Core Analysis

Permeability to air and helium-injection porosity measurements were conducted at ambient on all selected twelve samples. Permeability to air (Kair) and porosity values ranged from 0.210 to 3650 mD and 10.2 to 27.0% respectively. Grain density values ranged from 2.65 to 2.70 g/cc.

A sub-set of six samples was selected to undergo porosity and permeability measurements at four additional incremental confining stresses of 1500, 1782, 2500 and 3000 psi. Results from these measurements are tabulated in page 2-3.

Electrical Properties

The six samples selected for porosity and permeability measurements at multiple confining stresses also underwent formation resistivity factor (FRF) measurements.

Cementation exponent “m” values, measured at 1782 psi NOBP, ranged between 1.54 to 1.76. The average “m” was 1.65.

Cation exchange capacity (CEC) analyses were performed on all six sample trim-ends by the wet chemistry method on crushed sample. The recorded CEC values ranged from 2.01 to 8.30 meq/100g.

Capillary Pressure

Four samples, with permeability to air (Kair) values ranging from 0.740 to 295 mD were selected to undergo centrifuge air-brine capillary pressure tests. At the maximum air-brine capillary pressure of 350 psi, immobile water saturation (Swi) values ranged from 13.4 to 44.6 percent pore volume (% PV).

Graphical summary of air permeability vs immobile water saturation (Swi) indicate the expected relationship of increasing Swi with decreasing permeability.

Residual Gas Saturation and Relative Permeability

Two types of gas displacement tests were utilised in this study :

- Centrifuge water displacing gas relative permeability tests (representing a “forced” imbibition scenario where capillary/gravity forces dominate in the reservoir) yielded the most optimistic values of residual gas saturation ranging from 5.2 to 12.8% PV.
- The simple counter-current imbibition tests (representing “true” imbibition) yielded more pessimistic values of residual gas saturation ranging from 23.1 to 33.4% PV.

Utilising data from the centrifuge water-gas (end-point) analysis, full relative permeability water-displacing-gas curves were derived using the MAK correlation (Ref : “Practical Approach to Determine Residual Gas Saturation and Gas-Water Relative Permeability” by H.Mulyadi, R.Amin and A. F. Kennaird, SPE 71523, 2001).

Grain size analysis

Grain size determinations by sieve analysis were conducted on five selected sample trim-ends. The dominant grain-size is in the 90-1000 micron region. The median grain size is between 90 and 125 microns.

INTRODUCTION

This report contains the final results of the Special Core Analyses study performed on selected core plug samples from the Well : Casino-2. This study was initiated by Andy Pietsch of Santos Limited (Santos).

The test programme involved :

- CT-Scanning of selected core plugs
- Porosity and permeability measurements at ambient and multiple net overburden pressures
- Formation factor at net overburden pressure (NOBP)
- Cation exchange capacity (CEC) by wet chemistry method
- Centrifuge water-displacing –gas relative permeability (end-point)
- Water-gas relative permeability (full-curves) derived from centrifuge water-gas relative permeability (end-point)
- Residual gas saturation by counter-current imbibition (CCI)
- Air-brine drainage capillary pressure by centrifuge
- Grain size analysis

Selected core plug samples for the SCAL programme were received from Amdel on 18th November 2002.

Although sample #18 passed the screening stage, it was omitted from the subsequent SCAL programme as remnant mercury droplets were seen in this sample. This sample was subsequently replaced with sample #8.

At Santos's request, trim-ends of samples #1 (1763.18m), #10 (1765.80m), #25 (1772.88m), #30 (1774.43m) and #50 (1780.46m) were forwarded to Santos's offices for a petrographic study, on 27th November 2002.

The simulated formation brine salinity used for this SCAL study was 14,100 ppm (Santos's e-mail dated 20th November 2002).

The request for additional tests (air-brine capillary pressure and residual gas, Sgr, determinations by counter current imbibition method) was confirmed in an e-mail from Santos on 23rd January 2003.

Preliminary results from the completed analyses were reported on an on-going basis with all preliminary results forwarded by 20th March 2003.

The white light core plug images presented in Appendix 3 were not requested for this study but we found these useful especially in conjunction with the CT-images. For this study, these are offered at no cost to Santos.

SECTION 2
SAMPLE IDENTIFICATION AND BASE DATA

Sample Identification and Base Data

Sample no.	Depth (m)	At Ambient		Grain Density (gm/cc)	SCAL TESTS
		Kair (md)	Porosity (%)		
6	1764.61	21.3	19.9	2.66	Kphi at NOBP, electricals, CEC
8	1765.13	2150	21.5	2.65	Kphi at NOBP, electricals, CEC (replacement for #18)
11	1766.10	0.330	12.2	2.67	Kphi at NOBP, electricals, CEC
12	1766.40	*	*	*	Backup
13	1766.70	274	25.4	2.67	KwKg, CCI, air-brine Pc
14	1767.05	0.210	10.2	2.68	KwKg and sieve analysis
15	1767.36	74.3	21.2	2.69	KwKg, CCI, air-brine Pc, sieve analysis
18	1768.47	*	*	*	Rejected - Droplets of mercury noted in sample
20	1769.14	0.736	13.0	2.65	KwKg, CCI, air-brine Pc, sieve analysis
21	1769.40	*	*	*	Backup
22	1769.70	3.84	15.0	2.65	Kphi at NOBP, electricals, CEC
24	1770.35	876	27.0	2.66	Kphi at NOBP, electricals, CEC
30	1774.43	3650	20.8	2.69	KwKg
32	1774.97	*	*	*	Backup
33	1775.30	13.4	17.6	2.68	KwKg, CCI, air-brine Pc, sieve analysis
34	1775.62	232	23.2	2.70	Kphi at NOBP, electricals, CEC

* Analysis / measurement not requested or performed.

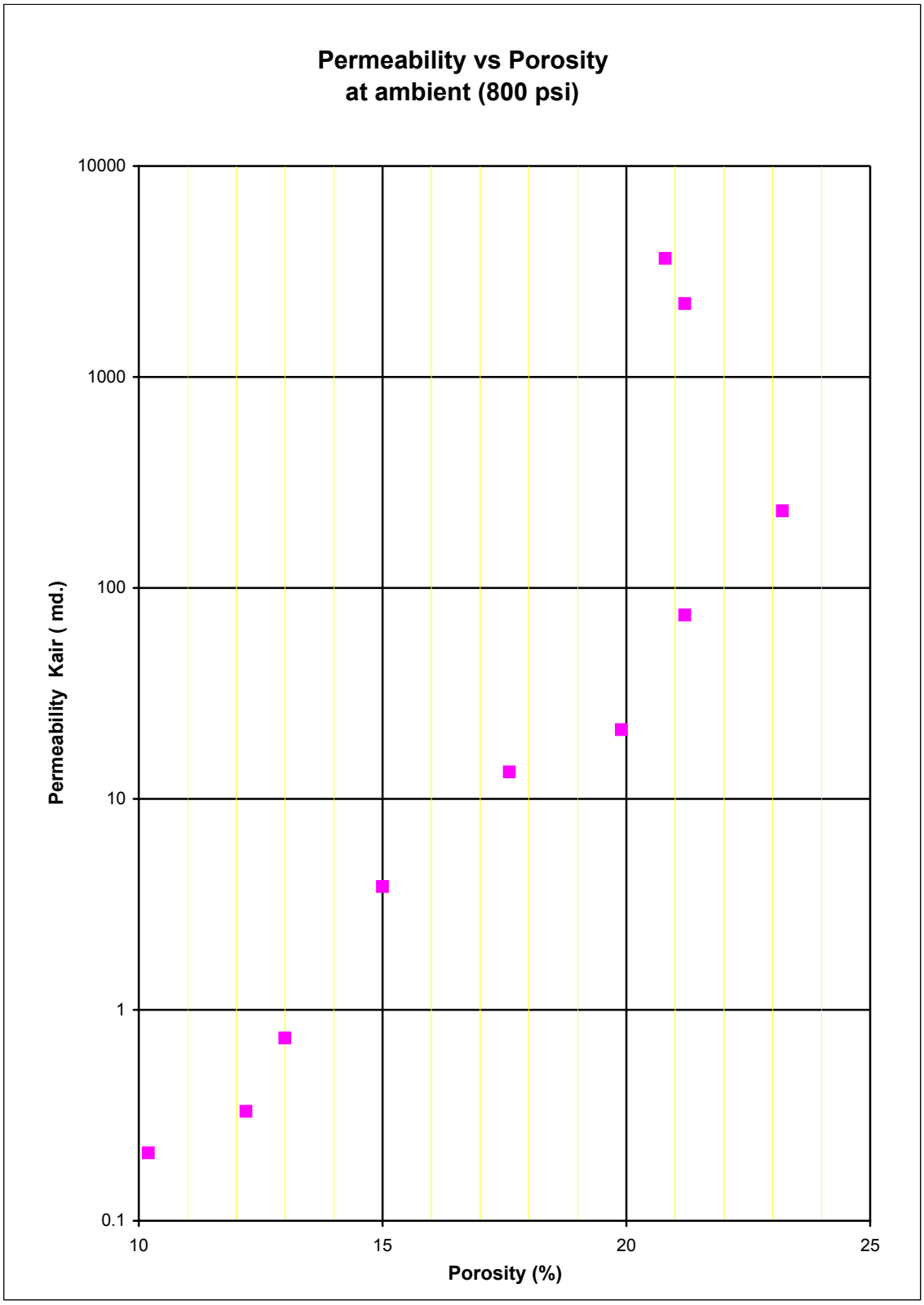
Permeability vs Porosity
at ambient (800 psi)
Permeability Kair (md.)
10000
1000
100
10
1
0.1
10
15
20
25
Porosity (%)

POROSITY, PERMEABILITY AND GRAIN DENSITY

Multiple Hydrostatic Confining Pressures

SMPL NO.	DEPTH (m)	GD (g/cc)	800 psi NOBP			1500 psi NOBP			1782 psi NOBP			2500 psi NOBP			3000 psi NOBP		
			PERMEABILITY		POROSITY	PERMEABILITY		POROSITY	PERMEABILITY		POROSITY	PERMEABILITY		POROSITY	PERMEABILITY		POROSITY
			Kinf (mD)	Kair (mD)	(%)	Kinf (mD)	Kair (mD)	(%)	Kinf (mD)	Kair (mD)	(%)	Kinf (mD)	Kair (mD)	(%)	Kinf (mD)	Kair (mD)	(%)
6	1764.61	2.66	18.4	21.3	19.9	17.4	20.2	19.6	17.2	19.9	19.5	16.7	19.3	19.3	16.4	19.0	19.2
8	1765.13	2.65	2120	2150	21.5	2070	2100	21.4	2050	2080	21.4	2030	2060	21.3	2020	2040	21.2
11	1766.10	2.67	0.228	0.330	12.2	0.126	0.204	11.8	0.105	0.175	11.7	0.075	0.133	11.5	0.064	0.119	11.4
22	1769.70	2.65	3.05	3.84	15.0	2.79	3.50	14.7	2.72	3.40	14.6	2.59	3.23	14.4	2.53	3.14	14.4
24	1770.35	2.66	863	876	27.0	844	859	26.7	839	852	26.6	828	842	26.5	822	835	26.4
34	1775.62	2.70	224	232	23.2	218	226	22.9	216	224	22.9	213	221	22.7	211	219	22.6

SECTION 3
ELECTRICAL PROPERTIES

Formation Resistivity Factor at a NOBP (1782 psi)

Sample no.	Depth (m)	K air at NOBP (mD)	Porosity (%)	FRF	Cementation exponent "m"
6	1764.61	19.9	19.5	13.6	1.60
8	1765.13	2080	21.4	12.7	1.65
11	1766.10	0.175	11.7	27.0	1.54
22	1769.70	3.40	14.6	25.4	1.68
24	1770.35	852	26.6	10.2	1.76
34	1775.62	224	22.9	12.1	1.69

Average "m" (forced regression, a = 1.0) = 1.65

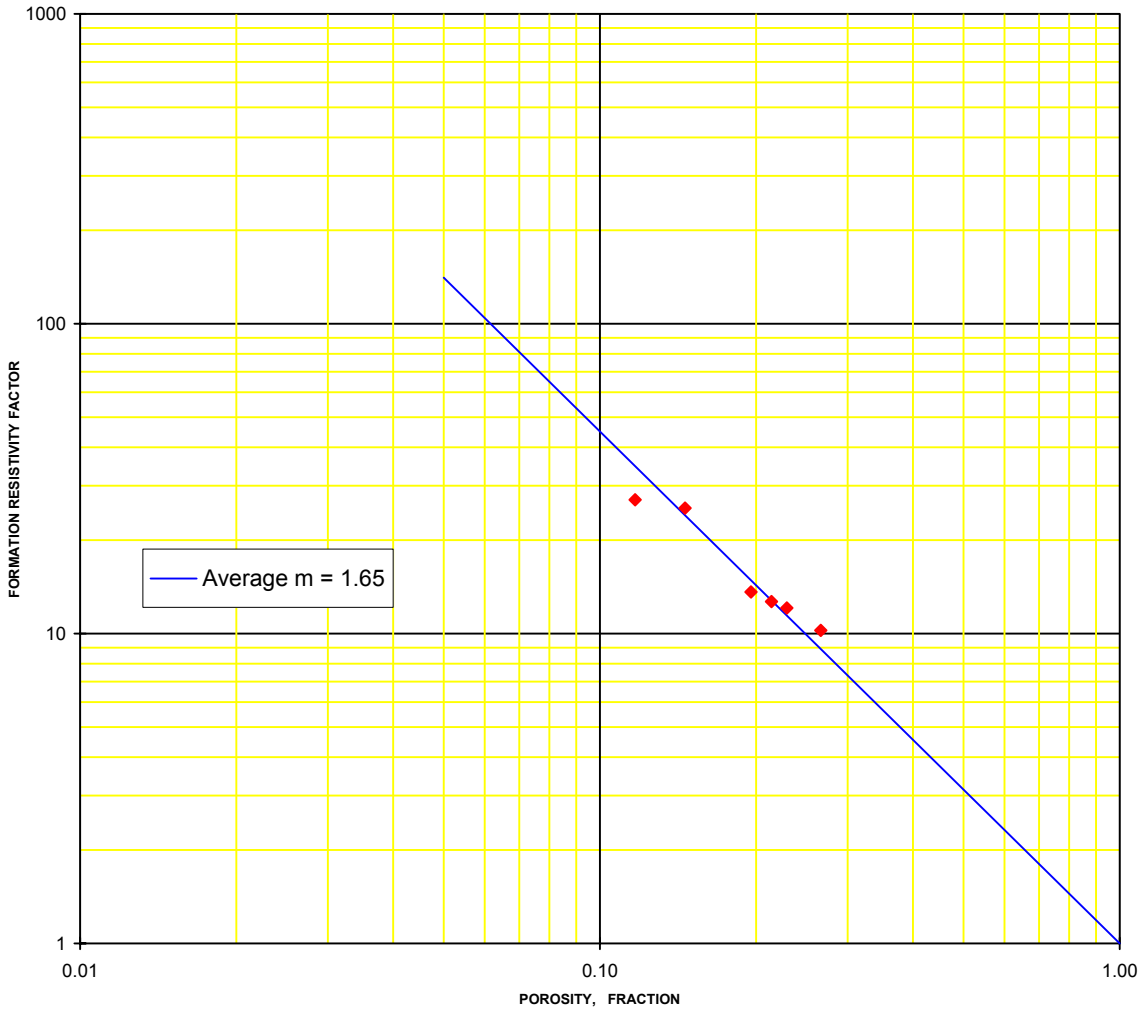

Cation Exchange Capacity by Wet Chemistry Method

Sample no.	Depth (m)	Permeability to air at NOBP (mD)	Porosity at NOBP (%)	CEC (meq/100 g)	Grain density (g/cc)
6	1764.61	19.9	19.5	7.52	2.66
8	1765.13	2080	21.4	2.01	2.65
11	1766.10	0.175	11.7	8.30	2.67
22	1769.70	3.40	14.6	5.29	2.65
24	1770.35	852	26.6	3.28	2.66
34	1775.62	224	22.9	4.47	2.70

CEC analysis conducted on core plug trim-ends.

SECTION 4
CAPILLARY PRESSURE

Summary of air-brine capillary pressure at ambient by centrifuge

Sample No.	Depth (m)	Kair* (mD)	Porosity* (%)	AIR - BRINE CAPILLARY PRESSURE (psi)								
				0	2	5	10	25	50	100	200	350
				END-FACE WATER SATURATION Sw (%pv)								
13	1766.70	295	25.6	100	52.2	37.6	28.9	22.7	19.0	15.8	14.1	13.4
15	1767.36	126	23.1	100	64.6	43.0	34.2	30.3	27.7	25.3	23.1	21.5
20	1769.14	0.740	13.3	100	100	100	90.5	75.4	65.7	57.2	49.9	44.6
33	1775.30	15.7	18.4	100	100	69.7	61.9	52.9	46.9	41.1	37.6	35.2

* Kair and porosity values were re-determined on re-cleaned samples prior to centrifuge air-brine Pc tests.

Water saturation (Swi) vs permeability to air

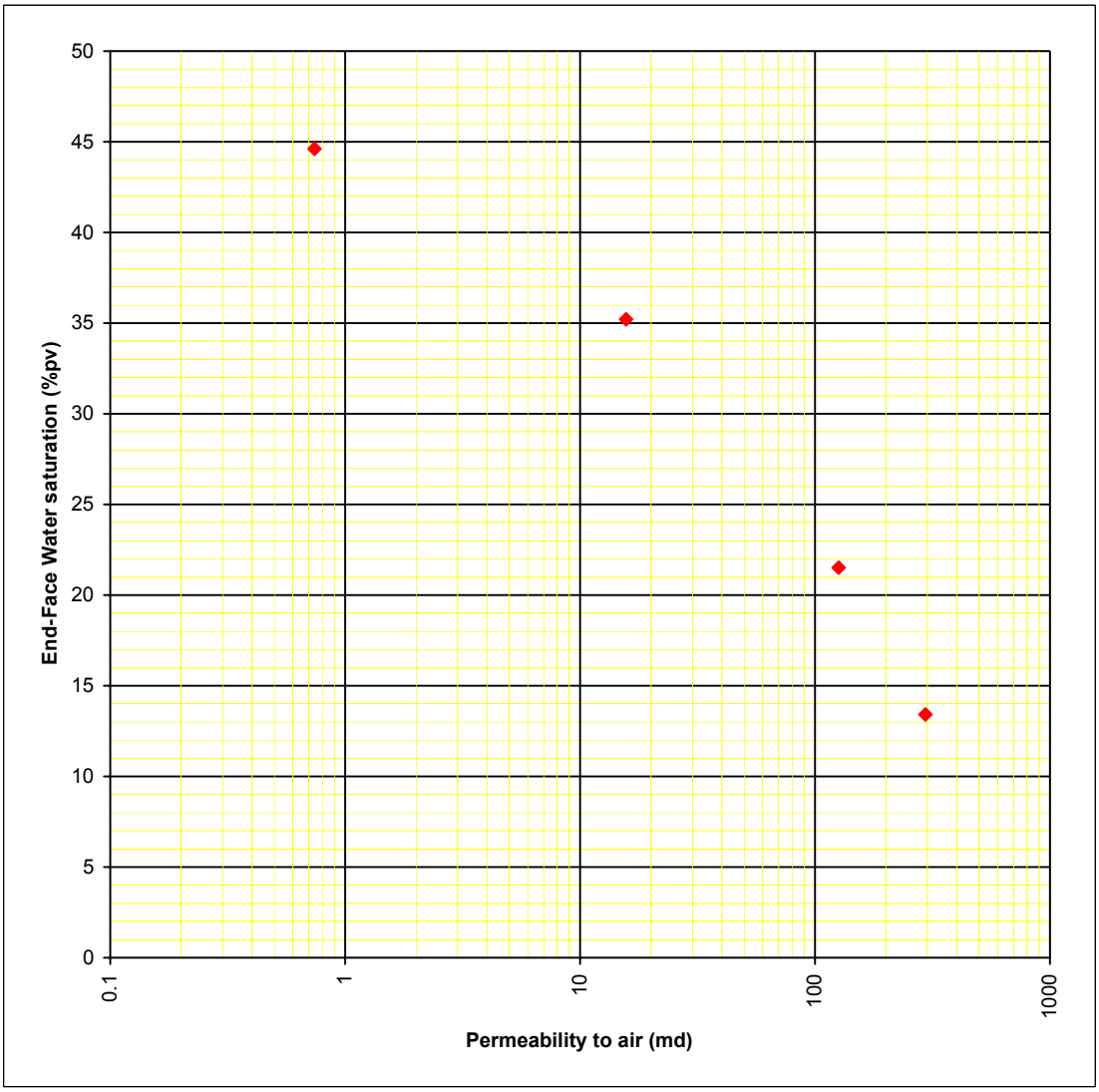

Air-brine Capillary Pressure by Centrifuge at Ambient

Sample no.	Depth (m)	Air permeability (mD)	Porosity (%)
13	1766.70	295	25.6

Capillary pressure (psi)	End face Water saturation (%pv)
0	100
2	52.2
5	37.6
10	28.9
25	22.7
50	19.0
100	15.8
200	14.1
350	13.4

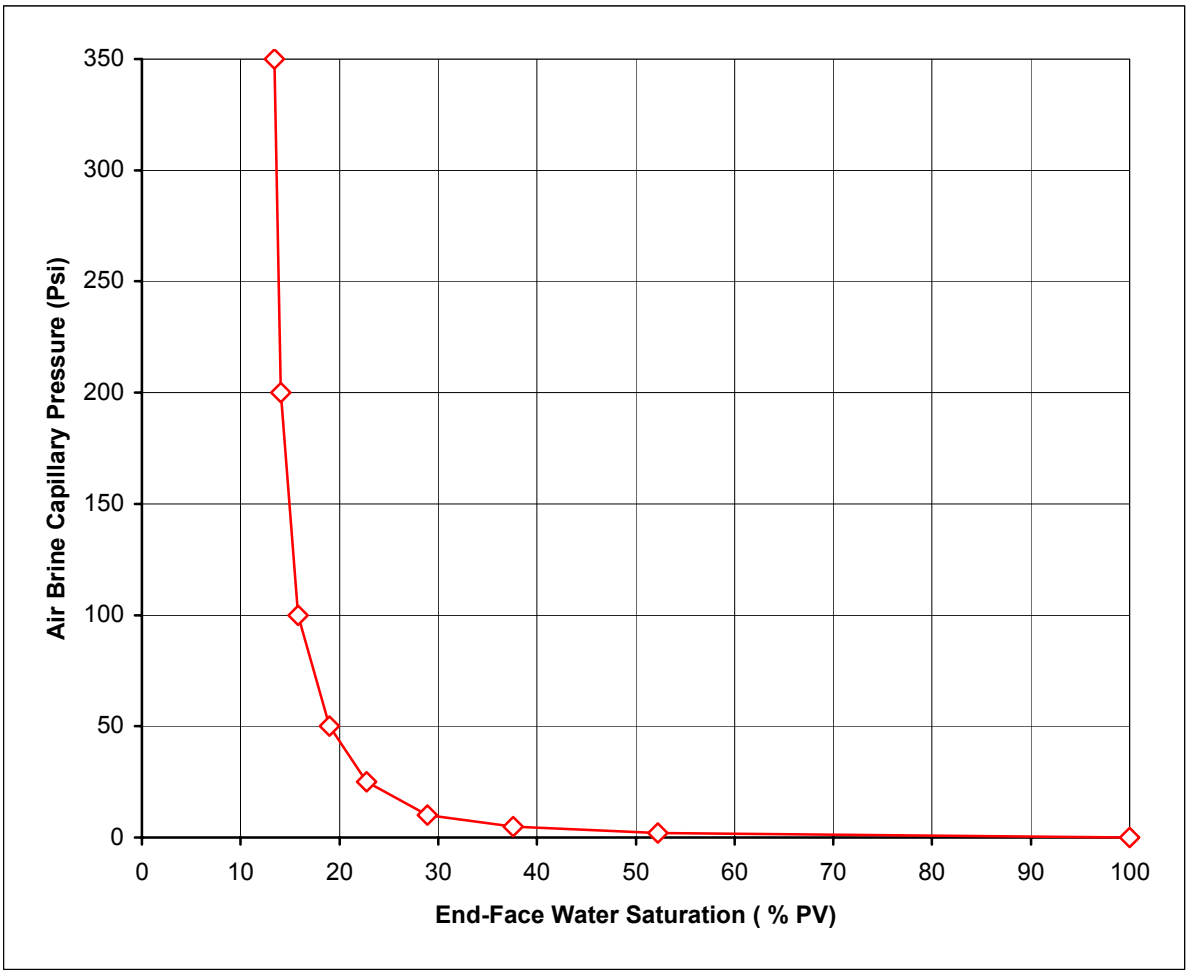

Air-brine Capillary Pressure by Centrifuge at Ambient

Sample no.	Depth (m)	Air permeability (mD)	Porosity (%)
15	1767.36	126	23.1

Capillary pressure (psi)	End face Water saturation (%pv)
0	100
2	64.6
5	43.0
10	34.2
25	30.3
50	27.7
100	25.3
200	23.1
350	21.5

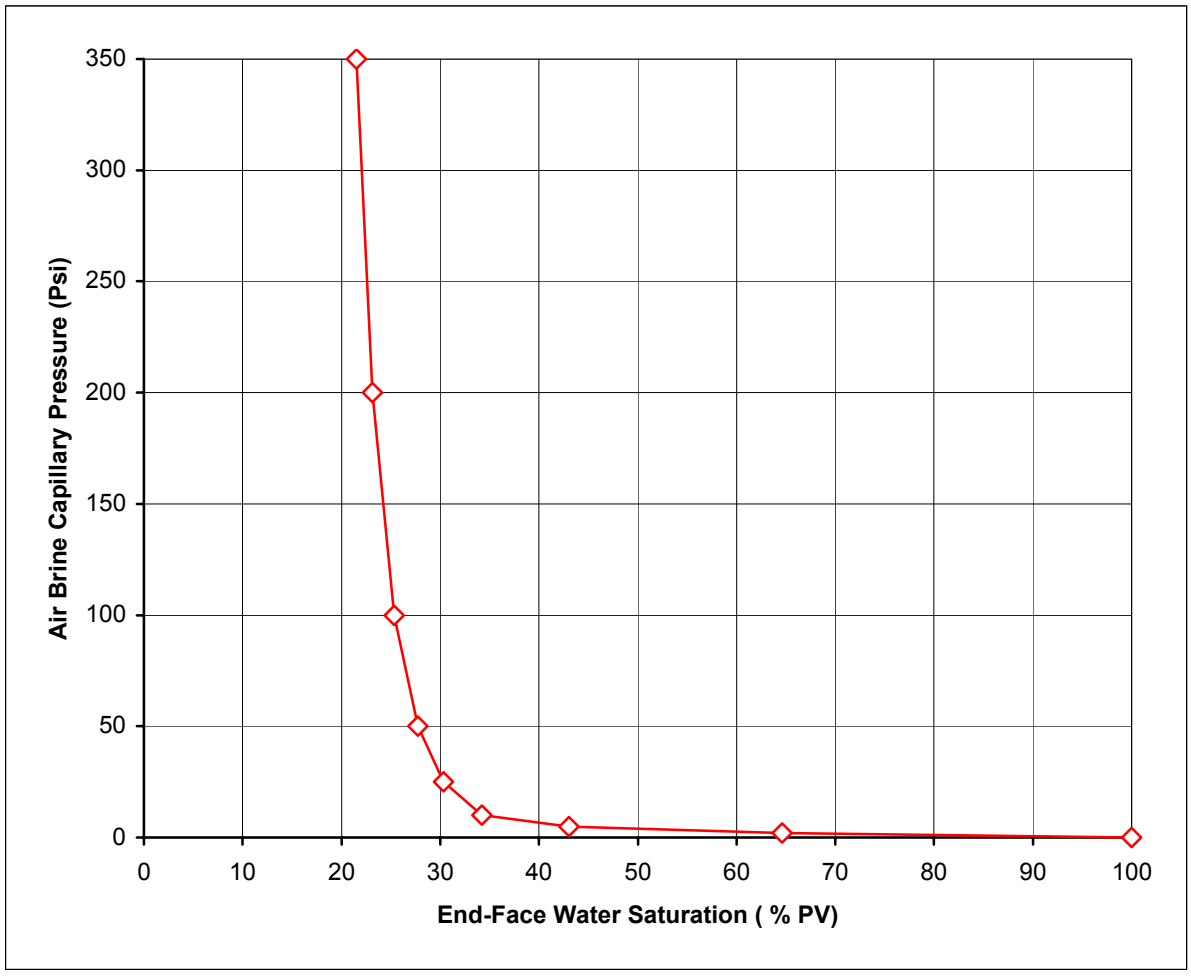

Air-brine Capillary Pressure by Centrifuge at Ambient

Sample no.	Depth (m)	Air permeability (mD)	Porosity (%)
20	1769.14	0.740	13.3

Capillary pressure (psi)	End face Water saturation (%pv)
0	100
2	100
5	100
10	90.5
25	75.4
50	65.7
100	57.2
200	49.9
350	44.6

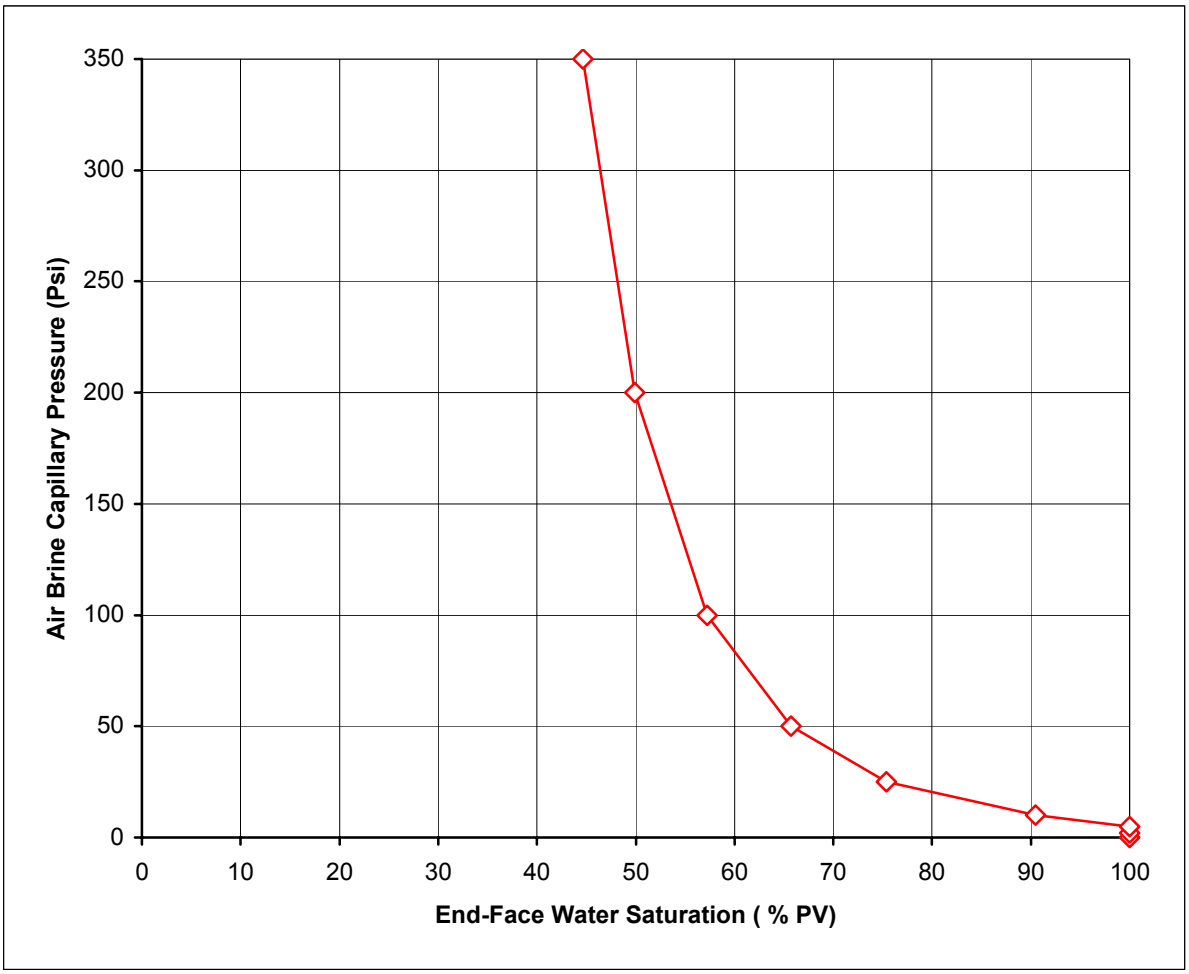

Air-brine Capillary Pressure by Centrifuge at Ambient

Sample no.	Depth (m)	Air permeability (mD)	Porosity (%)
33	1775.30	15.7	18.4

Capillary pressure (psi)	End face Water saturation (%pv)
0	100
2	100
5	69.7
10	61.9
25	52.9
50	46.9
100	41.1
200	37.6
350	35.2

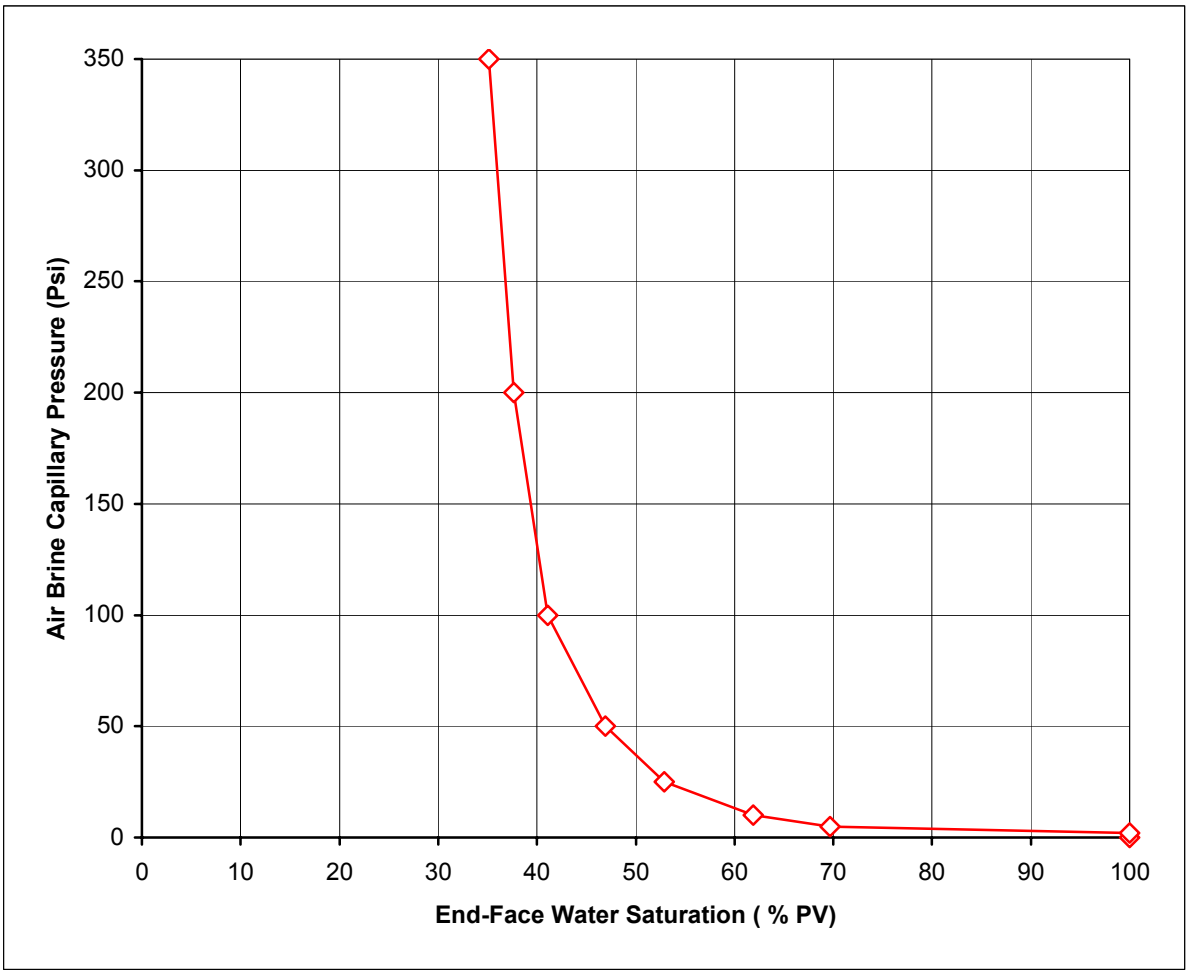

SECTION 5
RESIDUAL GAS SATURATION AND RELATIVE PERMEABILITY

RESIDUAL GAS SATURATION

Counter-Current Imbibition Method

Sample Id.	Depth, (m)	Kair * (mD)	Porosity * (%)	Initial Liquid Saturation, % PV	Initial Gas Saturation % PV	Residual Gas Saturation % PV	Gas Displaced % PV
13	1766.70	295	25.6	20.0	80.0	32.8	47.2
15	1767.36	126	23.1	20.0	80.0	33.4	46.6
20	1769.14	0.740	13.3	45.0	55.0	23.1	31.9
33	1775,30	15.7	18.4	25.0	75.0	26.5	48.5

* Kair and porosity values were re-determined on re-cleaned samples prior to CCI tests.

Summary of the WATER-GAS relative permeability by centrifuge (end-point) analysis results determined at ambient conditions.

Sample No.	Depth (m)	Kair at ambient (mD)	Porosity at ambient (%)	INITIAL CONDITIONS			TERMINAL CONDITIONS			
				Swi (% pv)	Initial gas in place (% pv)	Kgas at Swi (mD)	Sgr (% pv)	Gas Recovery (% pv)	Gas Recovery (% IIGP)	Kw at Sgr (mD)
13	1766.70	274	25.4	23.3	76.7	234	11.7	65.0	84.7	71.5
14	1767.05	0.210	10.2	71.8	28.2	0.058	5.2	23.0	81.6	0.008
15	1767.36	74.3	21.2	24.1	75.9	72.1	12.3	63.6	83.8	17.5
20	1769.14	0.736	13.0	47.8	52.2	0.343	8.1	44.1	84.5	0.102
30	1774.43	3650	20.8	8.0	92.0	3183	12.8	79.2	86.1	1287
33	1775.30	13.4	17.6	40.2	59.8	11.4	7.4	52.4	87.6	4.84

WATER-GAS Relative Permeability Curves
(derived from centrifuge WATER-GAS end-point relative permeability)

Sample number	**13**
Depth, metres	**1766.70**
Permeability to air at ambient, mD	**274**
Porosity at ambient, %	**25.4**
Initial water saturation, %pv	**23.3**
Effective permeability to gas at Swi, at ambient, mD	**234**

* Relative to the effective permeability to gas at initial water saturation (at ambient).

Gas saturation (%pv)	Gas-water relative permeability ratio	Relative permeability to Water * (fraction)	Relative permeability to Gas * (fraction)
23.3	0.00E+00	0.00E+00	1.00E+00
33.3	9.31E-09	2.16E-09	2.32E-01
38.3	8.77E-07	1.11E-07	1.26E-01
43.3	2.79E-05	1.86E-06	6.66E-02
48.3	5.05E-04	1.68E-05	3.32E-02
53.3	6.67E-03	1.02E-04	1.53E-02
58.3	7.42E-02	4.74E-04	6.39E-03
63.3	7.78E-01	1.80E-03	2.31E-03
68.3	8.61E+00	5.85E-03	6.80E-04
73.3	1.17E+02	1.69E-02	1.45E-04
78.3	2.57E+03	4.40E-02	1.72E-05
83.3	2.11E+05	1.06E-01	5.02E-07
88.3	-	2.38E-01	-

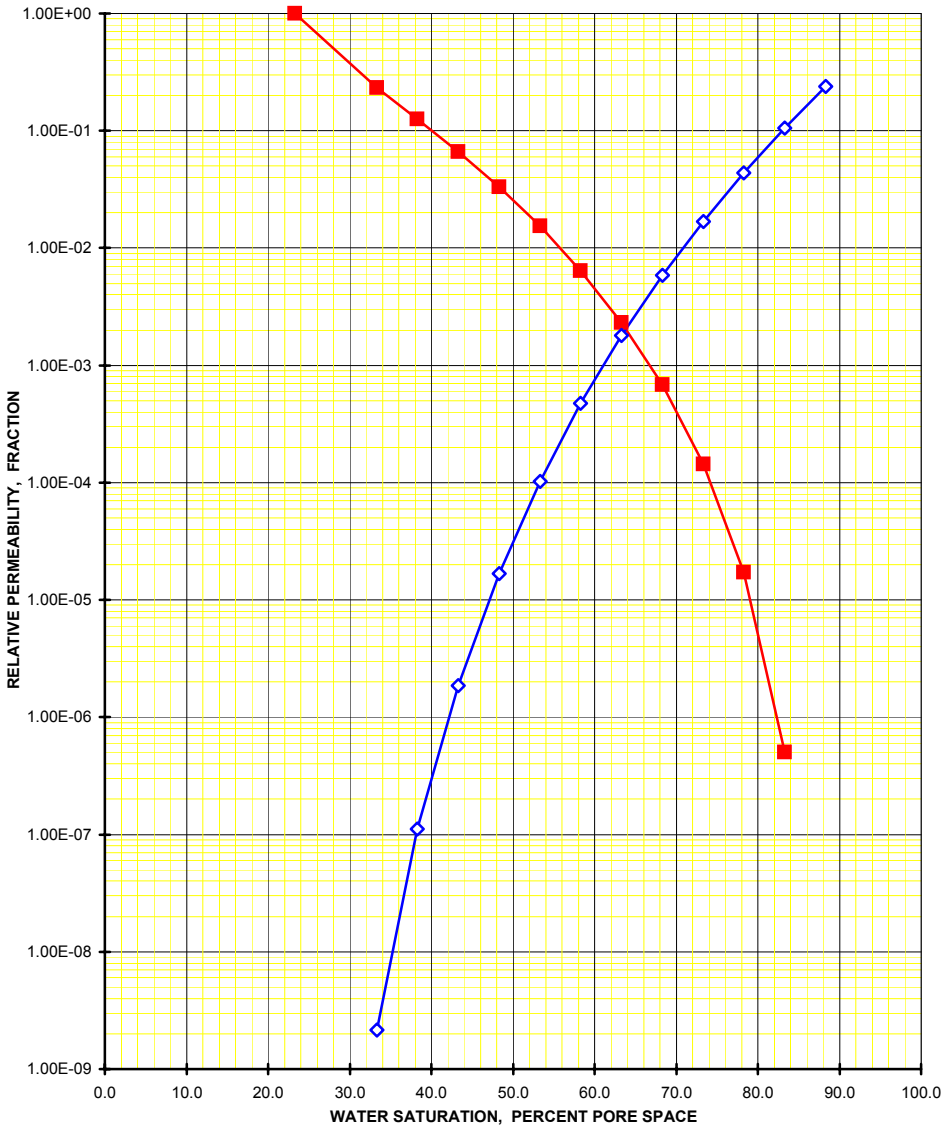

WATER-GAS Relative Permeability Curves
(derived from centrifuge WATER-GAS end-point relative permeability)

Sample number	**14**
Depth, metres	**1767.05**
Permeability to air at ambient, mD	**0.210**
Porosity at ambient, %	**10.2**
Initial water saturation, %pv	**71.8**
Effective permeability to gas at Swi, at ambient, mD	**0.058**

* Relative to the effective permeability to gas at initial water saturation (at ambient).

Gas saturation (%pv)	Gas-water relative permeability ratio	Relative permeability to Water * (fraction)	Relative permeability to Gas * (fraction)
71.8	0.00E+00	0.00E+00	1.00E+00
76.8	1.51E-03	9.88E-04	6.56E-01
81.8	4.34E-02	1.58E-02	3.64E-01
86.8	5.10E-01	8.01E-02	1.57E-01
91.8	6.02E+00	2.53E-01	4.20E-02
94.8	-	4.43E-01	-

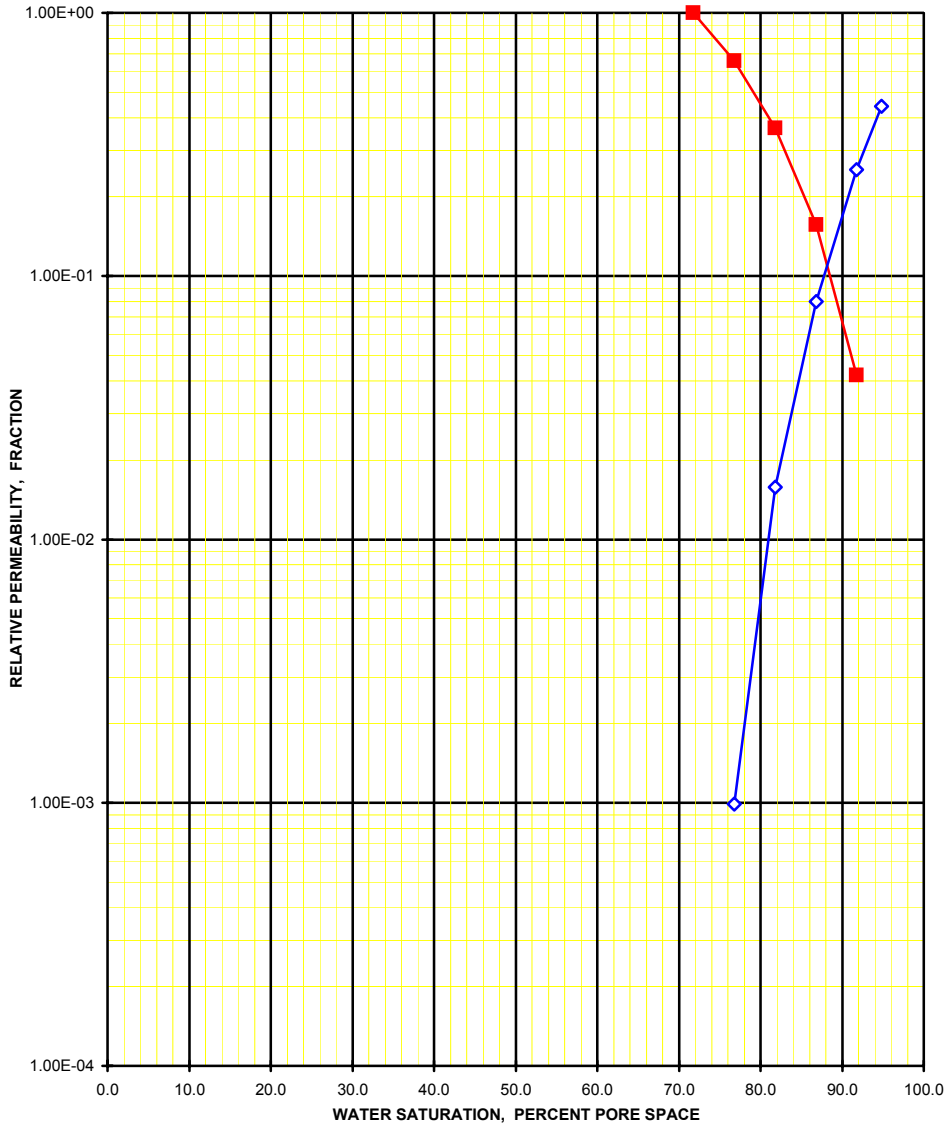

WATER-GAS Relative Permeability Curves
(derived from centrifuge WATER-GAS end-point relative permeability)

Sample number	**15**
Depth, metres	**1767.36**
Permeability to air at ambient, mD	**74.3**
Porosity at ambient, %	**21.2**
Initial water saturation, %pv	**24.1**
Effective permeability to gas at Swi, at ambient, mD	**72.1**

* Relative to the effective permeability to gas at initial water saturation (at ambient).

Gas saturation (%pv)	Gas-water relative permeability ratio	Relative permeability to Water * (fraction)	Relative permeability to Gas * (fraction)
24.1	0.00E+00	0.00E+00	1.00E+00
34.1	2.75E-08	6.14E-09	2.23E-01
39.1	2.14E-06	2.56E-07	1.20E-01
44.1	6.01E-05	3.71E-06	6.17E-02
49.1	9.97E-04	2.98E-05	2.99E-02
54.1	1.24E-02	1.66E-04	1.34E-02
59.1	1.33E-01	7.10E-04	5.34E-03
64.1	1.38E+00	2.51E-03	1.82E-03
69.1	1.57E+01	7.70E-03	4.92E-04
74.1	2.31E+02	2.10E-02	9.10E-05
79.1	6.38E+03	5.22E-02	8.18E-06
84.1	1.21E+06	1.20E-01	9.89E-08
87.7	-	2.10E-01	-

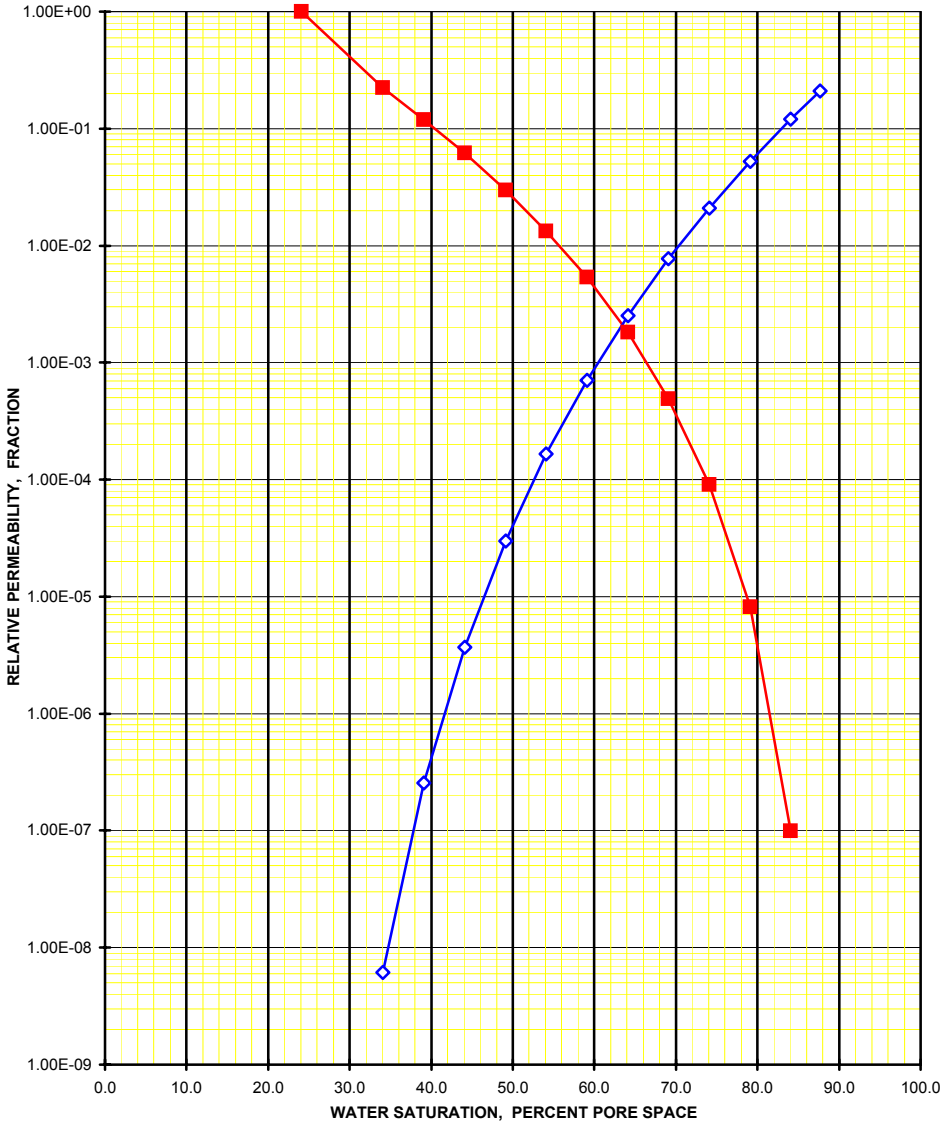

WATER-GAS Relative Permeability Curves
(derived from centrifuge WATER-GAS end-point relative permeability)

Sample number	**20**
Depth, metres	**1769.14**
Permeability to air at ambient, mD	**0.736**
Porosity at ambient, %	**13.0**
Initial water saturation, %pv	**47.8**
Effective permeability to gas at Swi, at ambient, mD	**0.343**

* Relative to the effective permeability to gas at initial water saturation (at ambient).

Gas saturation (%pv)	Gas-water relative permeability ratio	Relative permeability to Water * (fraction)	Relative permeability to Gas * (fraction)
47.8	0.00E+00	0.00E+00	1.00E+00
52.8	1.04E-04	8.42E-05	8.10E-01
57.8	2.14E-03	1.35E-03	6.30E-01
62.8	1.46E-02	6.82E-03	4.66E-01
67.8	6.64E-02	2.15E-02	3.25E-01
72.8	2.51E-01	5.26E-02	2.09E-01
77.8	9.01E-01	1.09E-01	1.21E-01
82.8	3.38E+00	2.02E-01	5.98E-02
87.8	1.53E+01	3.45E-01	2.25E-02
91.9	-	5.09E-01	-

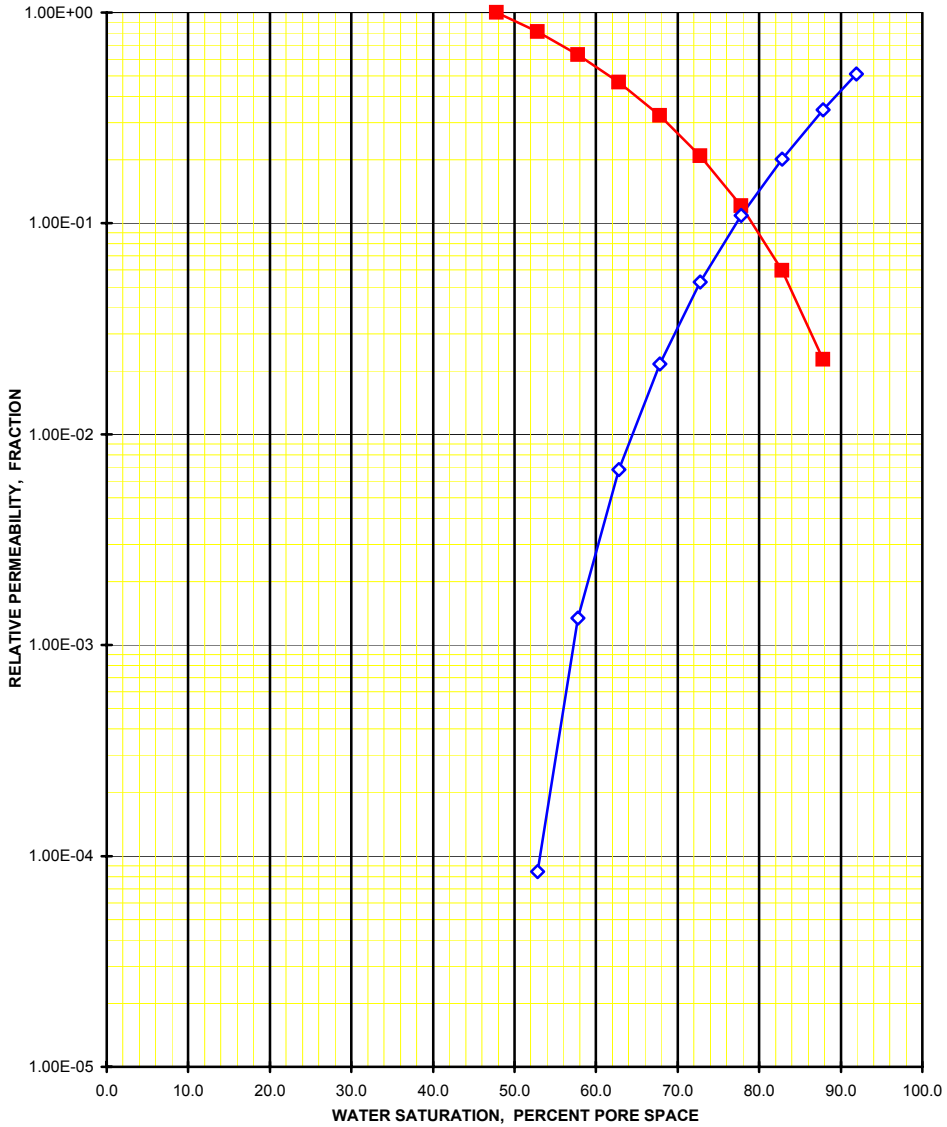

WATER-GAS Relative Permeability Curves
(derived from centrifuge WATER-GAS end-point relative permeability)

Sample number	**30**
Depth, metres	**1774.43**
Permeability to air at ambient, mD	**3650**
Porosity at ambient, %	**20.8**
Initial water saturation, %pv	**8.0**
Effective permeability to gas at Swi, at ambient, mD	**3183**

* Relative to the effective permeability to gas at initial water saturation (at ambient).

Gas saturation (%pv)	Gas-water relative permeability ratio	Relative permeability to Water * (fraction)	Relative permeability to Gas * (fraction)
8.0	0.00E+00	0.00E+00	1.00E+00
18.0	1.02E-08	6.51E-09	6.37E-01
23.0	3.90E-07	1.99E-07	5.11E-01
28.0	5.70E-06	2.31E-06	4.05E-01
33.0	4.94E-05	1.56E-05	3.17E-01
38.0	3.09E-04	7.51E-05	2.43E-01
43.0	1.56E-03	2.84E-04	1.82E-01
48.0	6.84E-03	9.03E-04	1.32E-01
53.0	2.72E-02	2.51E-03	9.24E-02
58.0	1.02E-01	6.26E-03	6.15E-02
63.0	3.75E-01	1.44E-02	3.83E-02
68.0	1.41E+00	3.06E-02	2.17E-02
73.0	5.83E+00	6.16E-02	1.06E-02
78.0	3.00E+01	1.18E-01	3.92E-03
83.0	2.92E+02	2.15E-01	7.35E-04
87.2	-	3.46E-01	-

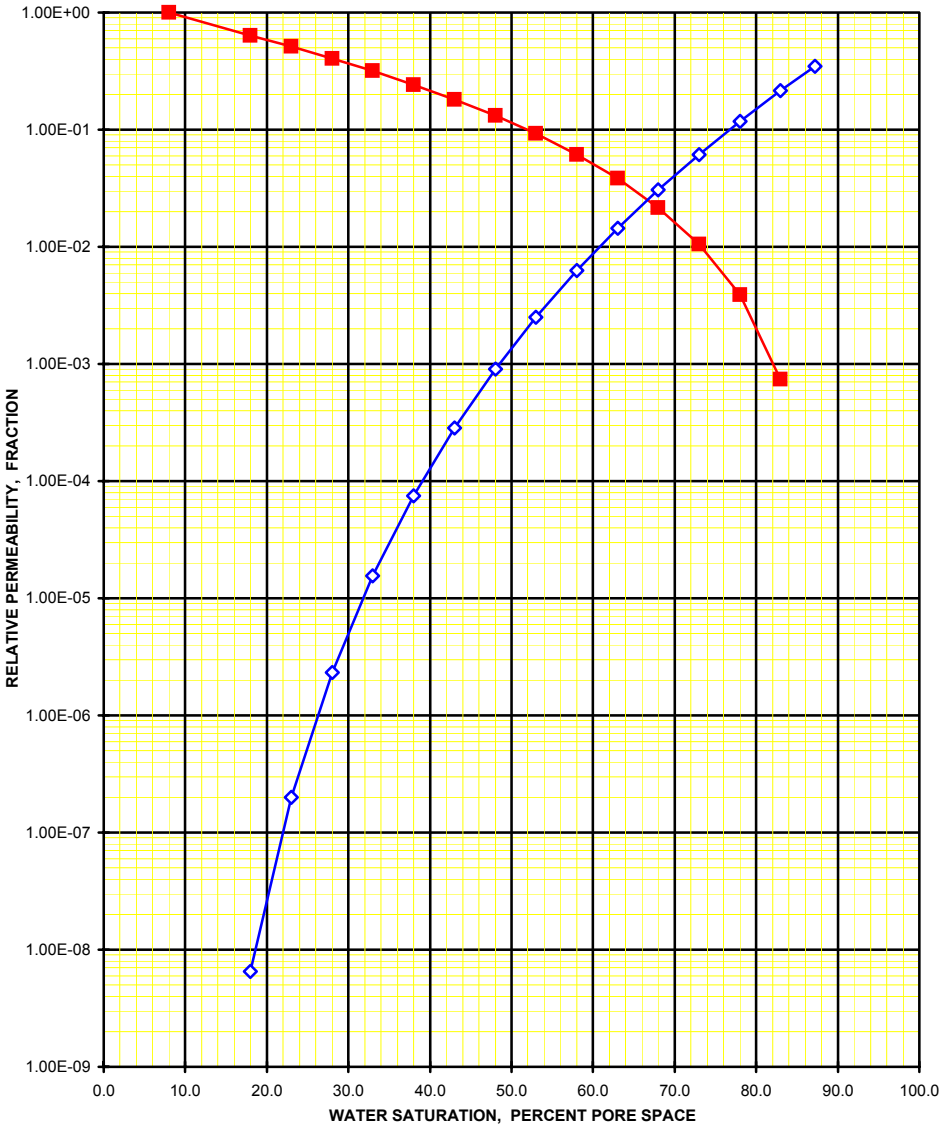

WATER-GAS Relative Permeability Curves
(derived from centrifuge WATER-GAS end-point relative permeability)

Sample number	**33**
Depth, metres	**1775.30**
Permeability to air at ambient, mD	**13.4**
Porosity at ambient, %	**17.6**
Initial water saturation, %pv	**40.2**
Effective permeability to gas at Swi, at ambient, mD	**11.4**

* Relative to the effective permeability to gas at initial water saturation (at ambient).

Gas saturation (%pv)	Gas-water relative permeability ratio	Relative permeability to Water * (fraction)	Relative permeability to Gas * (fraction)
40.2	0.00E+00	0.00E+00	1.00E+00
50.2	2.03E-06	5.97E-07	2.94E-01
55.2	9.04E-05	1.50E-05	1.66E-01
60.2	1.70E-03	1.51E-04	8.91E-02
65.2	2.09E-02	9.17E-04	4.39E-02
70.2	2.11E-01	4.04E-03	1.92E-02
75.2	2.05E+00	1.42E-02	6.94E-03
80.2	2.31E+01	4.25E-02	1.84E-03
85.2	4.27E+02	1.12E-01	2.63E-04
90.2	5.53E+04	2.68E-01	4.85E-06
92.6	-	3.95E-01	-

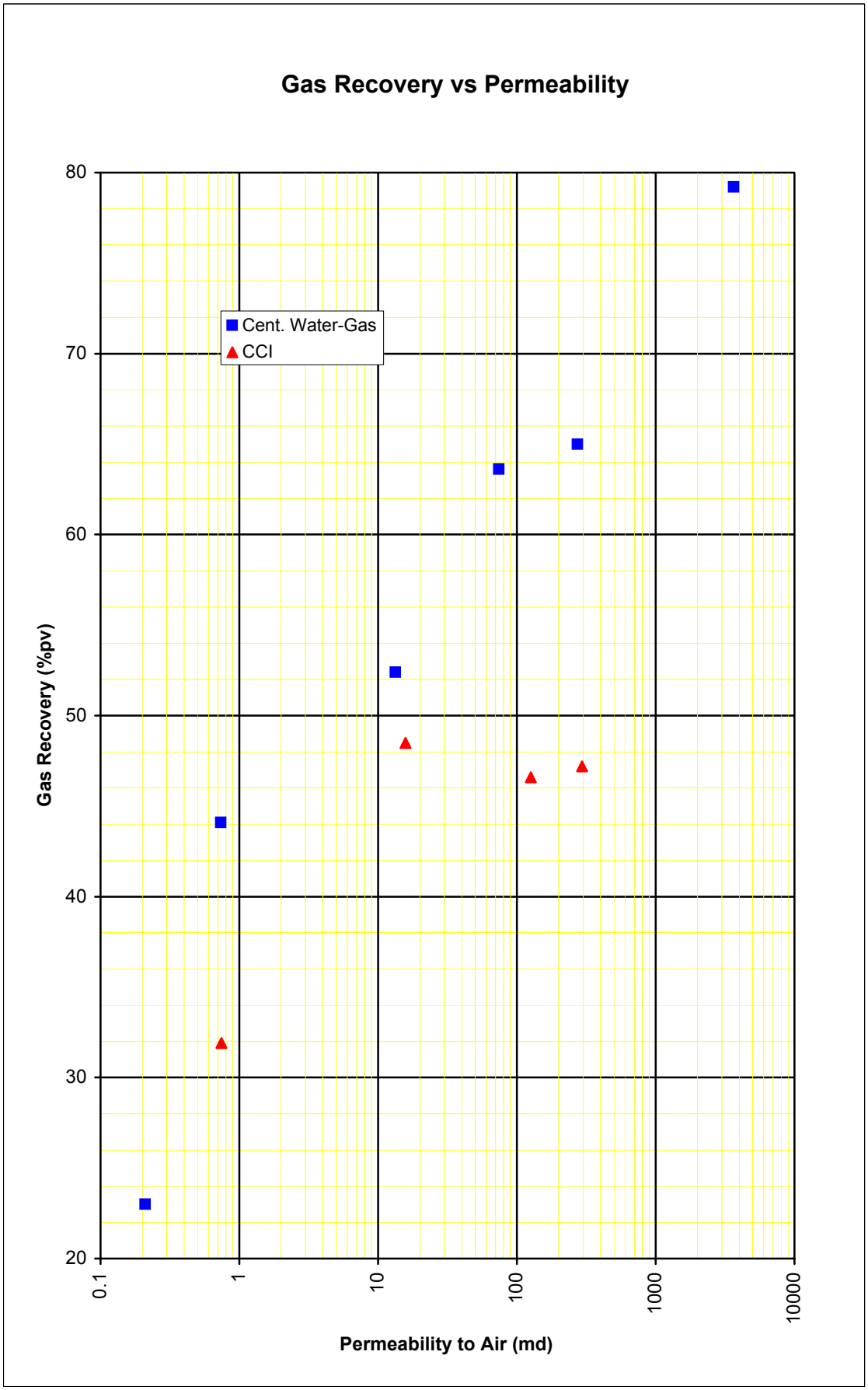
Gas Recovery vs Permeability
Cent. Water-Gas
CCI
Gas Recovery (%pv)
80
70
60
50
40
30
20
0.1
1
10
100
1000
10000
Permeability to Air (md)

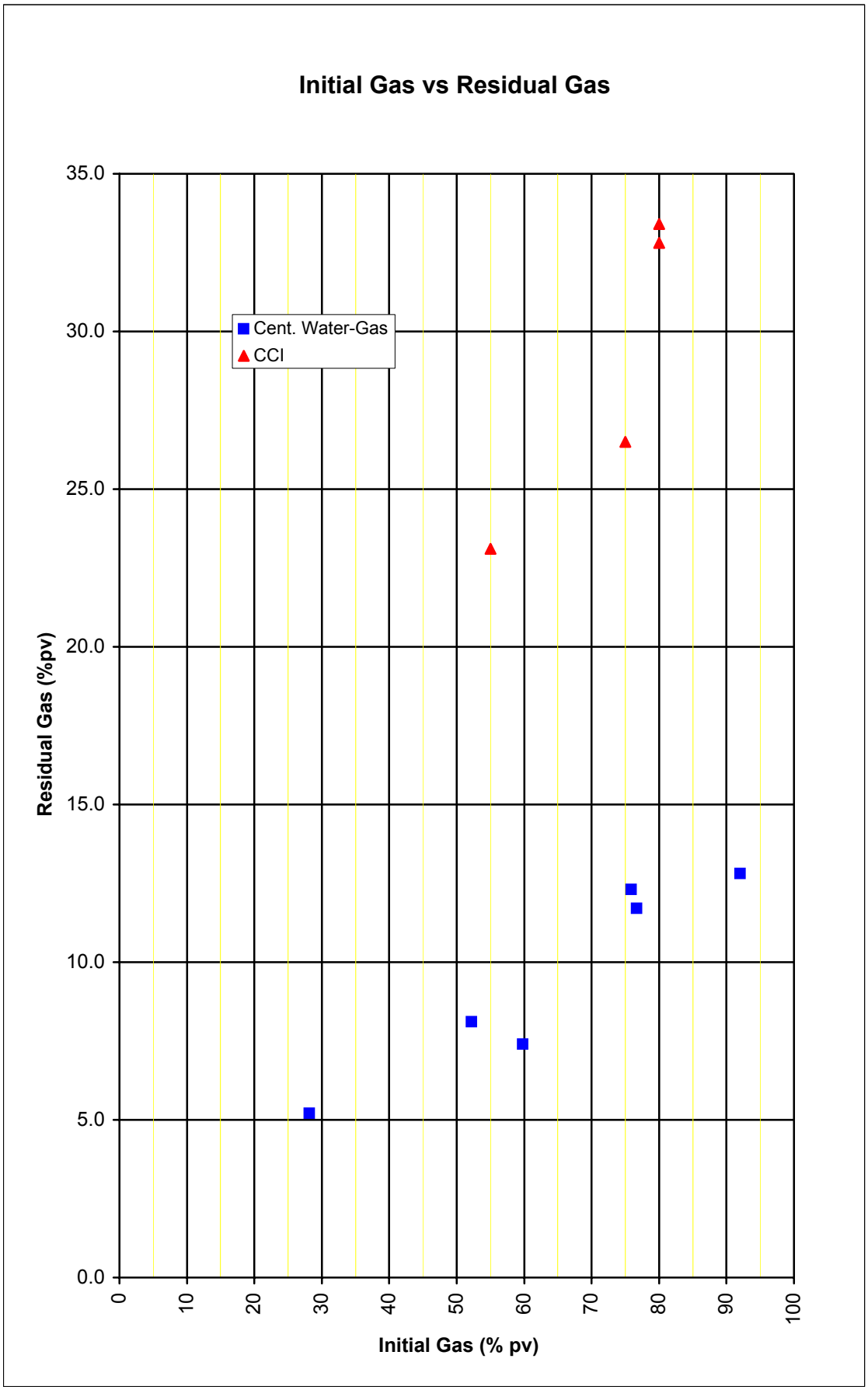
Initial Gas vs Residual Gas
Cent. Water-Gas
CCl
Residual Gas (%pv)
Initial Gas (% pv)
35.0
30.0
25.0
20.0
15.0
10.0
5.0
0.0
0
10
20
30
40
50
60
70
80
90
100

SECTION 6
SIEVE ANALYSIS

Sample 14
Well Casino 2
Depth (m) 1767.05

Results of a sieve analysis.

Sieve size (microns)	Percentage grain size (wt %)	Cumulative percent (wt %)
500	24.09	24.09
250	13.79	37.88
125	21.66	59.53
90	11.66	71.19
63	11.26	82.45
45	7.05	89.51
<45	10.49	100.00

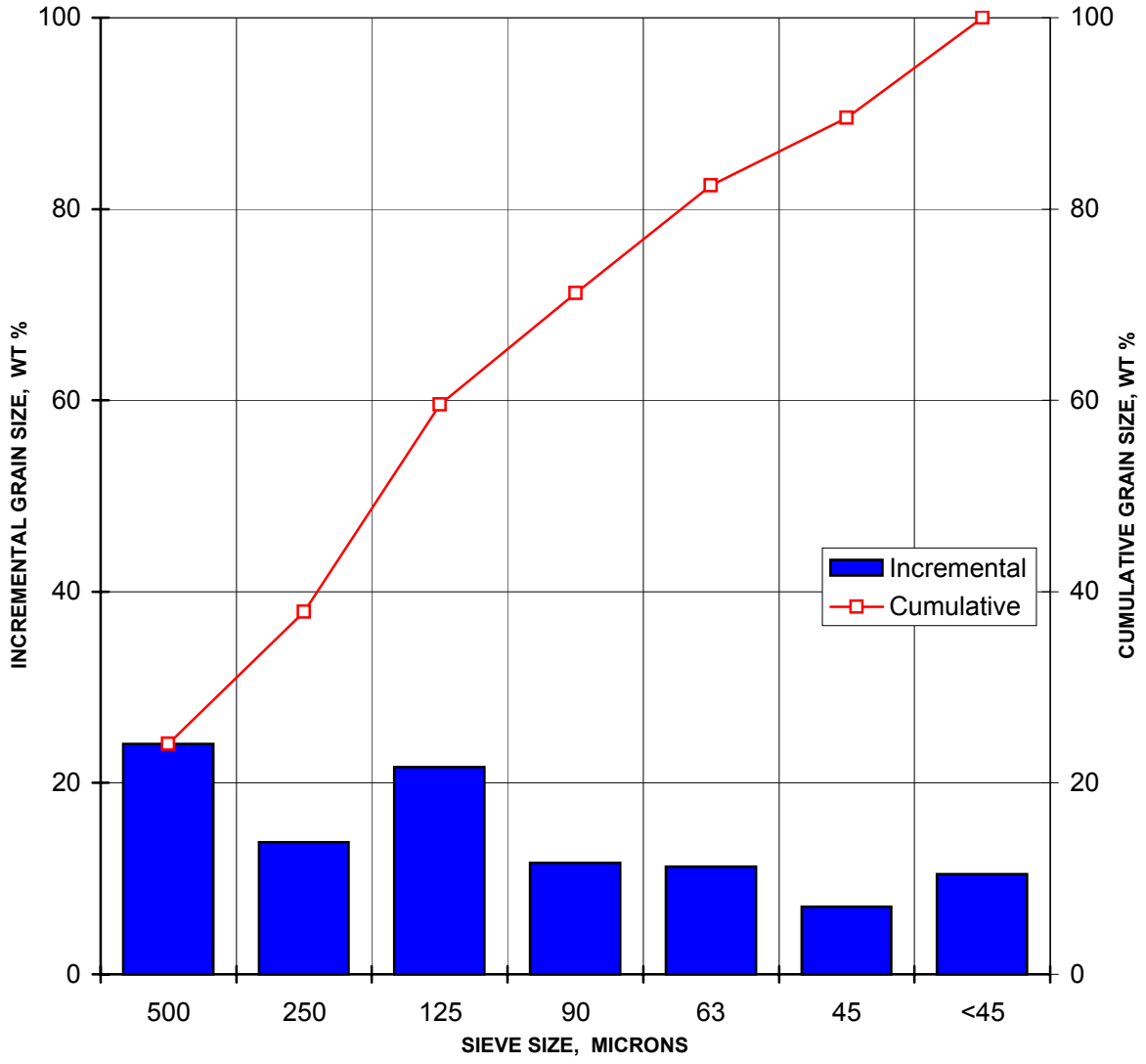

Sample 15
Well Casino 2
Depth (m) 1767.36

Results of a sieve analysis.

Sieve size (microns)	Percentage grain size (wt %)	Cumulative percent (wt %)
500	2.86	2.86
250	5.25	8.11
125	20.69	28.80
90	45.74	74.54
63	14.41	88.95
45	3.82	92.77
<45	7.23	100.00

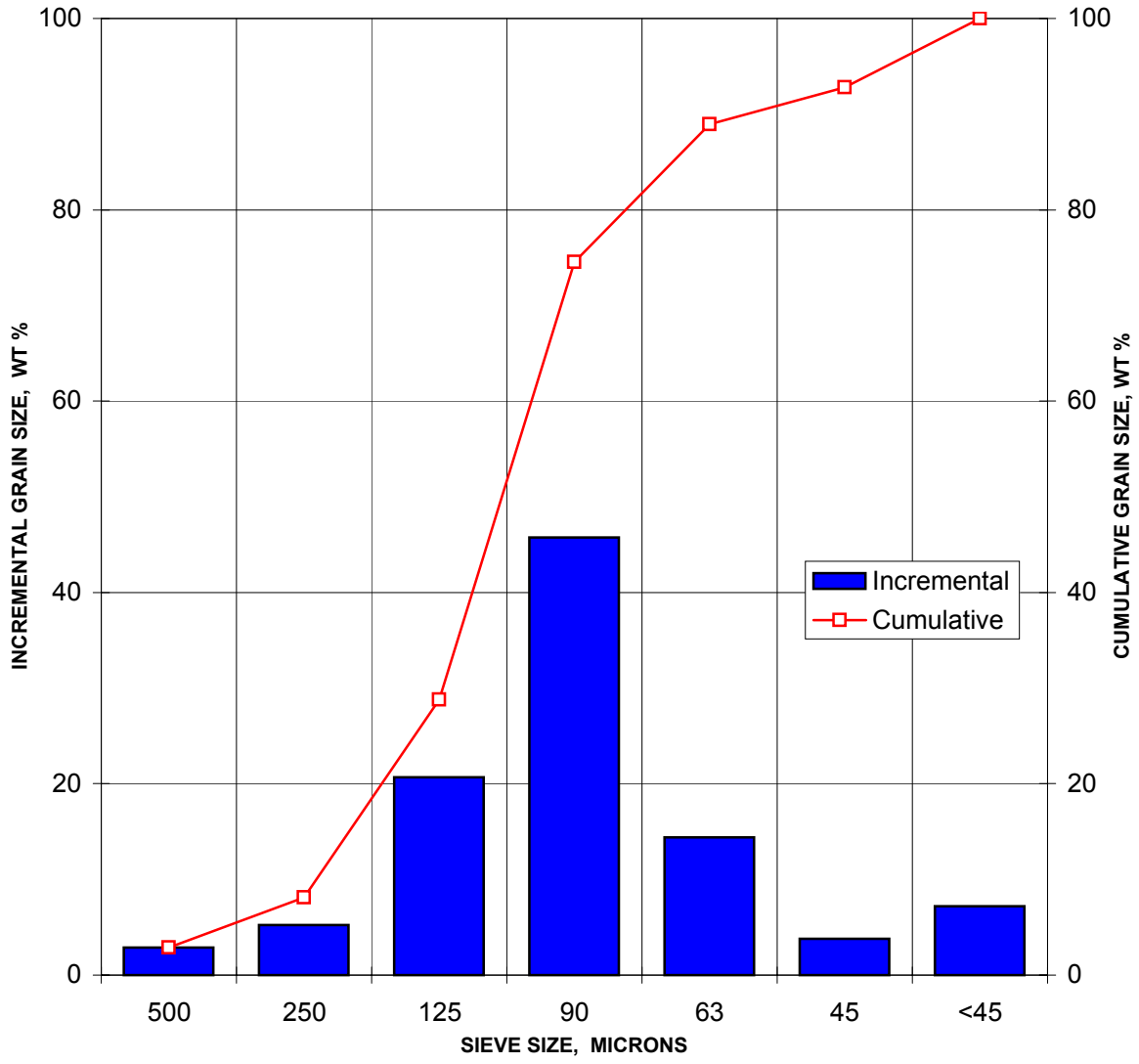

Sample 20
Well Casino 2
Depth (m) 1769.14

Results of a sieve analysis.

Sieve size (microns)	Percentage grain size (wt %)	Cumulative percent (wt %)
500	22.91	22.91
250	28.55	51.47
125	27.83	79.30
90	5.98	85.28
63	6.44	91.73
45	3.57	95.30
<45	4.70	100.00

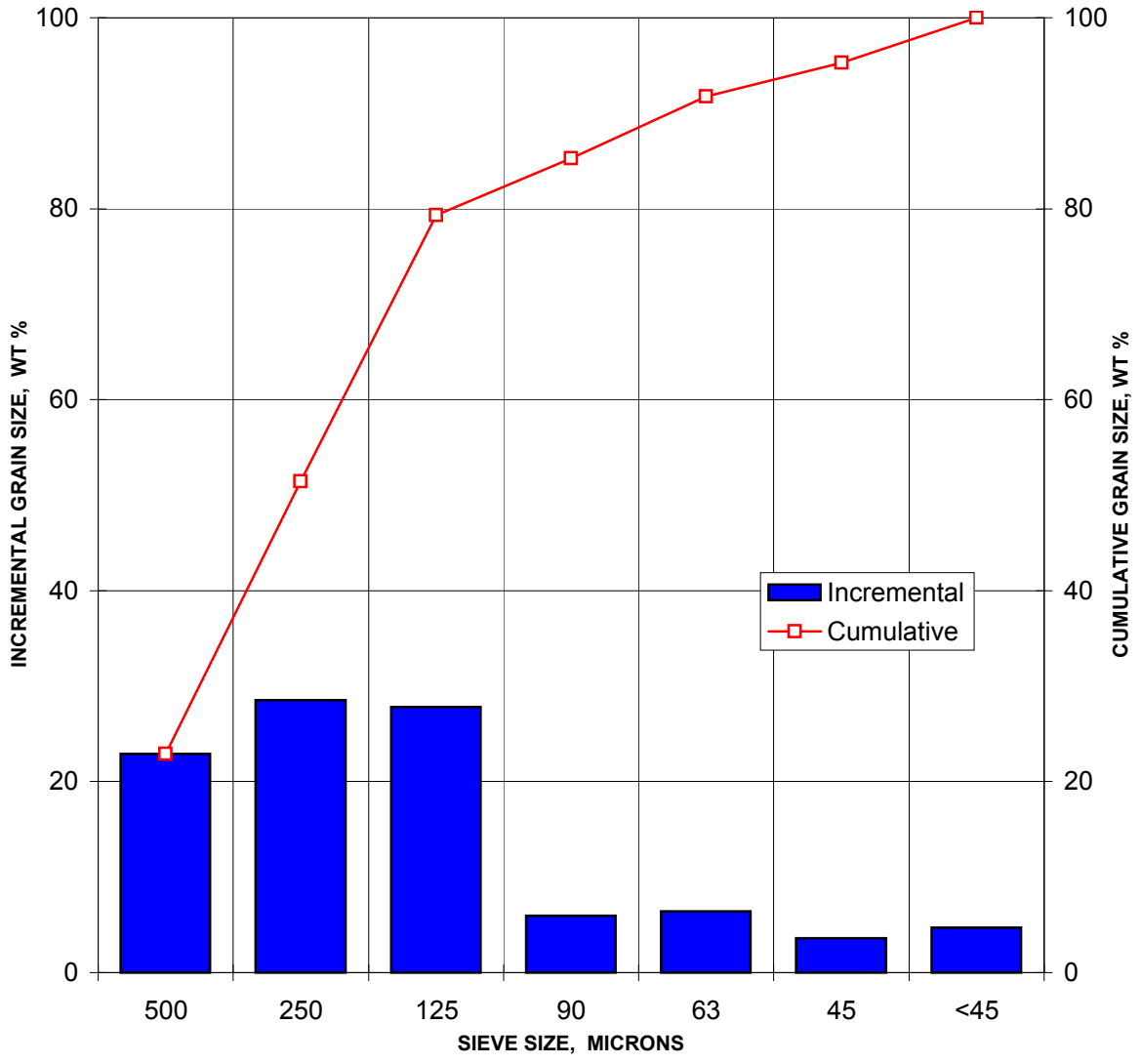

Sample 33
Well Casino 2
Depth (m) 1775.30

Results of a sieve analysis.

Sieve size (microns)	Percentage grain size (wt %)	Cumulative percent (wt %)
500	0.95	0.95
250	6.17	7.12
125	37.76	44.89
90	28.17	73.05
63	14.84	87.89
45	3.96	91.85
<45	8.15	100.00

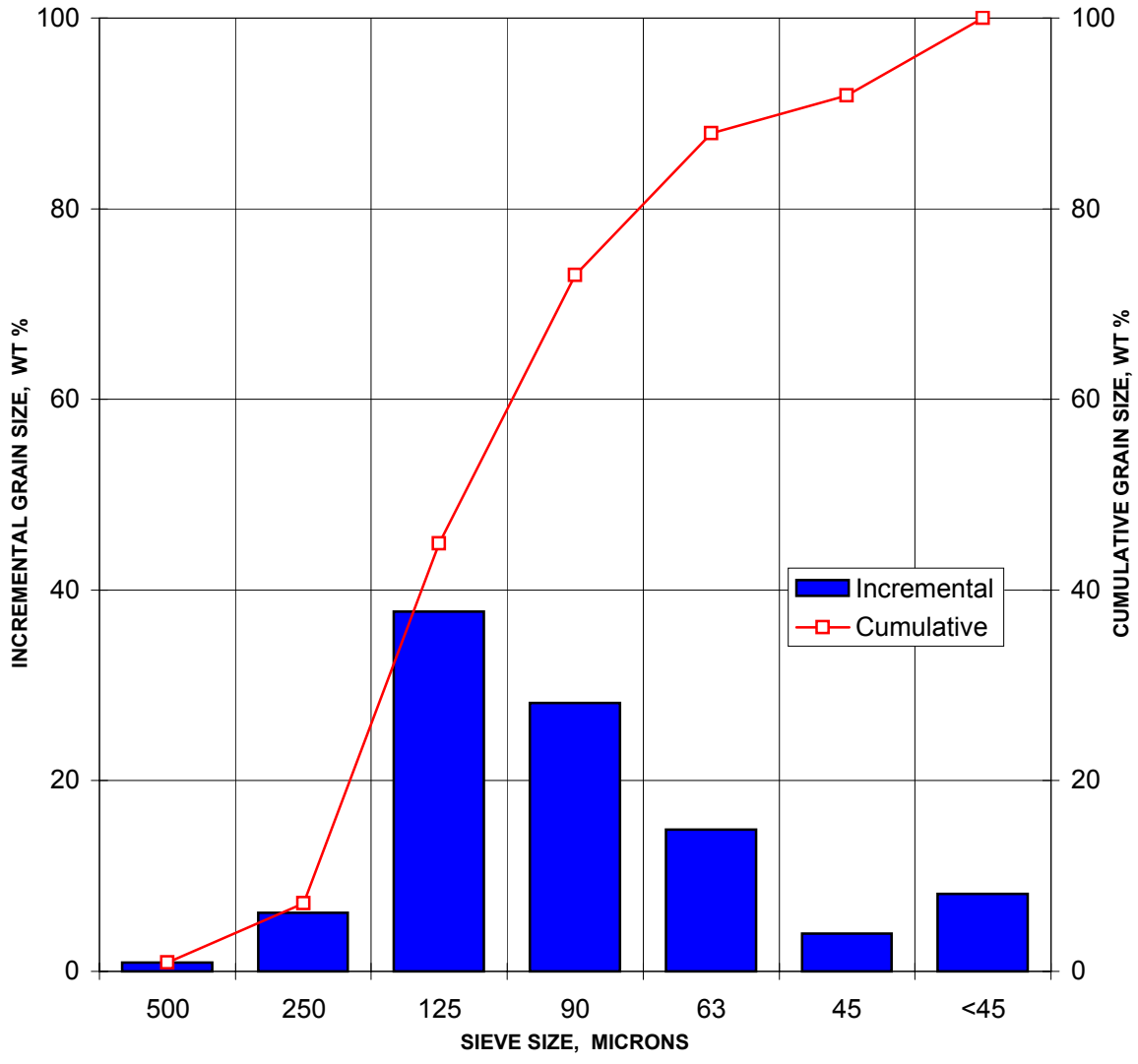

APPENDICES

APPENDIX 1
SUMMARY OF LABORATORY PROCEDURES

Summary of Laboratory Procedures

Sample Preparation

Selected core plug samples were received from Amdel on 18th November 2002 for a Special Core Analysis (SCAL) study. The samples had previously undergone routine core analysis measurements, conducted by Amdel, and thus cleaned and dried.

All samples selected for the study (twelve plus four backup samples) underwent visual and CT-screening to determine their suitability for further SCAL analyses.

After CT-screening, samples were re-dried in a convection oven at 95°C prior to porosity, permeability and grain density measurements.

Grain Volume and Grain Density

The weight, diameter and length of all samples were measured before they were processed through the Ultrapore™ porosimeter to determine grain volume. As a standard quality control measure, a calibration check plug was run after every ten samples. Grain density data was calculated from grain volume and sample weight data.

Permeability and Porosity

Permeability and pore volume measurements were made on all twelve core plug samples at 800 psi confining pressure in the CMS™300 automated core measurement system. A standard check plug was run with every five plug samples. Klinkenberg permeability (Kinf) values are obtained directly from the CMS™300, since it operates by unsteady-state principles. Porosity data was obtained by combining pore volumes from the CMS™300 with grain volumes from the Ultrapore™ porosimeter.

A sub-set of six samples was selected to undergo permeability and porosity measurements at four additional net overburden pressures (1500, 1782, 2500 and 3000 psi).

The complete routine core analysis results are presented on pages 2-1 and 2-3.

Saturation

All samples undergoing SCAL analyses were evacuated and pressure saturated with a simulated formation brine of 14,100 ppm concentration comprising 80% NaCl and 20% KCl. All samples were weighed after saturation to check measured pore volumes.

Formation Resistivity

Six samples were selected to undergo electrical properties measurements.

Each fully saturated sample was loaded into a coreholder at the reservoir equivalent NOBP (1782 psi) and the electrical resistivities measured on consecutive days until they were stable, indicating ionic equilibrium in the pore spaces. Formation factor (FRF) and cementation exponent ("m") values were then calculated.

The trimmed-ends of the plugs which underwent FRF and RI measurements were cleaned in methanol, dried at 60^{o}C in a non-humidified oven and then subjected to determinations of cation exchange capacity (CEC) using the ammonium acetate wet chemistry technique on crushed sample. These CEC values are used to calculate idealised "m*" and "n*" values using Waxman-Smits-Thomas equations.

Results from the electrical analysis are presented within SECTION 3 of this report.

Residual Gas Saturation by Centrifuge (Water Displacing Gas)

Six samples spanning the permeability range of 0.210 – 3650 mD were selected for residual gas saturation by centrifuge.

Each sample was initially evacuated and pressure saturated using the simulated formation brine. Samples were then desaturated in the centrifuge to attain immobile water saturation (Swi) at an equivalent air-brine capillary pressure of 350 psi.

The samples were next loaded into individual hydrostatic core-holders and effective gas permeabilities at immobile water saturation were determined at ambient conditions.

Brine-filled centrifuge cups were attached to the centrifuge coreholders and the samples were then spun at a maximum imbibition (equivalent to 350 psi), brine displacing air, capillary pressure to determine the end-point residual gas saturation (Sgr). The samples were removed from the centrifuge cups and the residual gas saturations were determined gravimetrically.

Each sample was then loaded into a hydrostatic core holder at ambient conditions. Brine was flowed through the samples and effective permeability to brine at Sgr was then determined.

Results from the water-gas relative permeability (end-point) by centrifuge are presented in SECTION 5 of this report.

Water Displacing Gas – Full Curve Simulation

From the centrifuge Kw/Kg end-point data and using the MAK Correlation full-curve data, were derived.

The derived water-gas relative permeability curves are presented in SECTION 5.

Residual Gas Saturation (Sgr) by Counter Current Imbibition (CCI)

In an e-mail dated, 23rd January 2003, Andries Steyn of Santos requested residual gas saturation (Sgr) by counter current imbibition (CCI) tests followed by centrifuge air-brine capillary pressure measurements on the six samples which had previously undergone residual gas saturation by centrifuge analysis. Two of the six samples (#14 and #30) were found unsuitable (damaged after earlier centrifuge analysis) hence they were eliminated from further analyses.

The selected samples were re-cleaned, dried, and the base data re-confirmed. Samples were then saturated with toluene and their saturated weights checked to confirm helium injection pore volume data.

Each sample was then evaporated to a gravimetrically-determined initial “liquid” saturation with the remaining void pore space being air (“gas”) filled. Initial liquid saturations were based on those derived during porous-plate desaturation prior to centrifuge residual gas saturation determinations.

The samples were suspended, in turn, in a tared cradle below a weigh balance in a container of toluene. As the toluene imbibed into the samples, gas displacement was recorded by increasing weight versus time. Equilibrium residual gas saturations were then calculated and these data are presented in SECTION 5 of the report.

Air-Brine Capillary Pressure by Centrifuge

After the CCI tests, all four samples were re-dried prior to saturation with the simulated formation brine. The samples were weighed after saturation to check measured pore volumes.

The selected samples were each loaded into individual centrifuge coreholders. Samples were spun at incremental rotational speeds effecting capillary pressure. Each speed (RPM) was maintained for a minimum of 24 hours until production was stable. The speed was then raised to the next higher speed. Volumes of brine produced were monitored using a stroboscope.

Capillary pressure and end-face saturation data were then calculated from the raw data using data reduction techniques developed by Hassler-Brunner and others. These results are presented within SECTION 4 of this report.

Sieve Analysis

Four samples were selected for sieve analysis for grain-size confirmation.

Each sample was dis-aggregated using a mortar and rubber pestle, weighed, and placed into a nest of pre-weighed sieves. Sieve screens were 500, 250, 125, 90, 63, and 45 microns. The sieve nest was placed in an ultra-sonic sifter for 15 minutes, 1 minute settling and then 15 minutes more sifting. Each sieve with its retained grains was then weighed to determine the percentage of the sample retained.

Results of all grain-size analysis are presented in SECTION 6 of the report.

APPENDIX 2
CT-SCAN DESCRIPTIONS

CT-Scanning

General Comments

The samples are well-indurated, moderately to poorly sorted quartz sandstones. The grain-size is variable within individual samples and from one sample to another; it ranges from fine to lower coarse, commonly with a few gains to granule-size. Glauconite and organic matter are common accessory features. Mudstone and siltstone may be a minor component and this is particularly evident in samples 14, 15, 32 and 33. All of the samples are inferred to show some evidence of bioturbation and this has resulted in variably confused attenuation fabrics.

Higher attenuation is mainly related to finer grain-size and the content of accessory pyrite (for example, mudstone tends to show relatively higher attenuation). However, high attenuation may be related to other cement phases with siderite particularly evident in sample 11. In contrast, localised low attenuation may be attributable to the presence of organic matter.

CT scans of sample #18 reveal numerous very high attenuation spots particularly concentrated along one end face. Visual binocular examination confirms that these spots are due to the presence of mercury droplets. Moreover, another five samples show traces of mercury contamination. It remains uncertain if sample #18 is the sole source of this contamination. Mercury cross contamination may have occurred whilst handling the samples given that droplets were observed amongst debris in the sample containers. Mercury is easily transferred via finger ridges from one sample to another.

X-ray CT images are presented with approximately the same image output parameters to facilitate visual comparisons from one sample to another. Average attenuation for the 16 samples ranges from 1281 to 2254 HU with a mean of 1584 HU.

Post CT scanning, all samples were examined and described by means of binocular microscopy and white light images recorded by low-resolution digital photography. The white light images record a view of one end face and longitudinal views rotated through 90° (i.e. essentially the same orientation as the CT scans). The images are presented in Appendix 3.

Individual sample descriptions are given in the following pages.

Sample Descriptions

Sample 6 (1764.61m) :

A very poorly sorted very fine to lower coarse-grained sandstone containing a trace of deformed granular glauconite and rare specks of organic matter. Coarser grained and finer grained domains are present in about equal proportions. The mottled attenuation fabric reflects these coarser and finer domains with the latter showing diffuse, slightly higher attenuation overall. This almost certainly is attributable to localised denser packing and associated cement, pyrite 'dust'. Granular pyrite, up to framework grain-size, is also present and there are minor pyritised organics. Lowest attenuation specks are probably related to organic matter (e.g. om) although in places larger open pores could be inferred. The overall attenuation fabric is reminiscent of bioturbation. The sample is moderately homogeneous overall and no defects are evident. Although not intersected on the CT scan, rare mercury droplets are noted on one end cut surface. Average CT Number 1610 HU, standard deviation 95 HU.

Sample 8 (1765.13 m) :

A generally upper medium to lower coarse-grained sandstone; it contains a minor finer-grained component with pyrite, and traces of disseminated glauconite. The slightly mottled attenuation fabric shows diffuse slightly higher attenuation in places and this is probably associated with concentrations of pyrite 'dust' (e.g. py) where there is finer grain-size. Disseminated grain-size spots of lowest attenuation are for the most part attributable to open pores (e.g. p) with a minor contribution from organic matter. The sample is essentially homogeneous and no defects are evident. Of note is the presence of several droplets of mercury on one end cut surface (binocular view through plastic-wrap). Average CT Number 1415 HU, standard deviation 76 HU.

Sample 11 (1766.10 m) :

A fine–grained sandstone featuring alternating mm-scale laminations containing vitrinitic organic matter (~10 %) and early-formed diagenetic siderite nodules (~7 %). Disrupting these laminations in places are disorganised patches inferred as burrows. Siderite (si) nodules give rise to localised spots of extremely high attenuation. Siderite clearly contributes to the relatively high average attenuation overall. The organic-rich layers would be anticipated to show lowest attenuation and this is in part the case (e.g. om), however, some of the organic matter is charged with pyrite. No defects are evident but the sample is poorly to moderately homogeneous overall. As with the previous sample, rare mercury droplets are present on both end cut surfaces. Average CT Number 2254 HU, standard deviation 298 HU.

Sample Descriptions (cont'd)

Sample 12 (1766.40 m) :

A laminated, generally upper fine to lower medium-grained sandstone containing a minor component of framework grains ranging to upper very coarse. Traces of glauconite and organic specks are apparent and there is some disturbance of layering and this is probably attributable to bioturbation. The attenuation fabric reveals that laminae are set slightly oblique to the plug axis. Higher attenuation of individual lamina is due to finer grain-size and associated pyrite 'dust'. The sample is moderately homogeneous and no defects are evident. Average CT Number 1458 HU, standard deviation 63 HU.

Sample 13 (1766.70 m) :

A mainly fine-grained sandstone with minor concentrations of larger framework grains to coarse sand-size. A trace of disseminated granular glauconite and organic specks is noted. The attenuation fabric is slightly mottled reflecting grain-size variation and slight concentrations of a cement phase, almost certainly pyrite 'dust'. A poorly defined layering is apparent but there is some disturbance of this feature probably attributable to bioturbation. The sample is moderately homogeneous and no defects are evident. Average CT Number 1382 HU, standard deviation 49 HU.

Sample 14 (1767.05 m) :

An argillaceous sandstone comprising disturbed, bioturbated sand packages disruptive of lesser sandstone, siltstone and mudstone laminae. The very fine to fine sands form about 50 % of the sample and are characterised by a chaotic fabric both visually and in X-ray attenuation. Very high attenuation speckling within these domains is associated with concentrations of pyrite (e.g. py), and rarely siderite, cement. High attenuation of the muddy layers (e.g. m) is also attributable to disseminated pyrite. Lowest attenuation streaks and threads is inferred as non-pyritised organic matter (e.g. om), a feature evident on visual examination. However, some of the lower attenuation spotting is almost certainly due to larger open pores; there is a trace of coarser framework grains in places. No defects are inferred but the sample is poorly homogeneous. Average CT Number 1981 HU, standard deviation 211 HU.

Sample Descriptions (cont'd)

Sample 15 (1767.36 m) :

A mainly upper very fine to lower fine grained sandstone comprising disturbed lenticular layers and probable burrows. The sand packages are variable in composition and range from relatively clean to argillaceous; minor mudstone is noted. The attenuation fabric reflects the presence of the argillaceous content mainly through higher attenuation of associated pyrite cement. This is most evident in the minor mudstone lenses (m). Ubiquitous slightly higher attenuation traces define sand layer boundaries and this too is evidence of pyrite, albeit in trace amounts. A distinctive diffuse patch of slightly higher attenuation is inferred as a burrow (b). A number of laminae contain flecks of vitrinitic organics. Associated with the organics are siderite nodules to 0.5 mm; these show spotty high attenuation (e.g.. si). Overall the sample is moderately homogeneous and no defects are evident. Average CT Number 1559 HU, standard deviation 181 HU.

Sample 18 (1768.47 m) :

A very poorly sorted, medium to very coarse-grained sandstone. A layered domain of diffuse slightly higher attenuation is the most conspicuous feature of the CT scans. This is inferred as a layer of finer grain-size with associated clays and pyrite 'dust'. Elsewhere, faint cross layering is apparent. Characterising these layers are trails of low attenuation spots; these are larger open pores. Highest attenuation spots within the attenuation fabric are most likely attributable to rare grain-size pyrite. However, very high attenuation spotting particularly evident along one of the cut faces is almost certainly due to the presence of mercury (Hg) droplets. The sample is moderately homogeneous and no defects are apparent. Average CT Number 1520 HU, standard deviation 229 HU.

Sample 20 (1769.14 m) :

A poorly sorted, generally medium-grained sandstone containing minor domains of coarse to very coarse framework grains. The mottled attenuation fabric reflects disorganised packages of compositionally variable sands. Domains with higher attenuation are indicative of smaller grain-size and greater content of pyrite 'dust'. Most porous cleaner sands show lower attenuation (e.g. ps). Disseminated spots of vitrinitic organic matter complicate the interpretation; some larger flecks show low attenuation (e.g. om) but others are pyritised (e.g. py). The sample is moderately homogeneous overall and no defects are evident. Although not apparent on the CT scans, traces of mercury are noted on the plug cut ends. Average CT Number 1736 HU, standard deviation 110 HU.

Sample Descriptions (cont'd)

Sample 21 (1769.40 m) :

A very poorly sorted, generally upper medium-grained argillaceous sandstone. It contains minor domains with framework grains ranging up to granule-size as well as silty trails charged with organic matter. The mottled attenuation fabric is reminiscent of bioturbation and features several patches of very high attenuation; these are domains of pyrite cemented sand (e.g. py). More diffuse slightly higher attenuation is derived from pyrite 'dust' associated with finer grain-size. The sample is moderately homogeneous and no defects are evident. Average CT Number 1672 HU, standard deviation 108 HU.

Sample 22 (1769.70 m) :

A poorly sorted, generally fine to medium-grained sandstone with minor concentrations of coarser framework grains grading to upper granule-size. The attenuation fabric is evenly mottled reflecting domains of compositionally variable sands. This fabric almost certainly is attributable to bioturbation. Diffuse domains of slightly higher attenuation are probably finer grained and contain associated pyrite 'dust'. Lowest attenuation spotting within generally lower attenuation domains is attributable to larger open pores. However, low attenuation also is due to the presence of organic matter traces (e.g. om). Some of the organic matter is pyritised (e.g. py). The sample is moderately homogeneous and no defects are evident. Average CT Number 1676 HU, standard deviation 130 HU.

Sample 24 (1770.35 m) :

An upper fine-grained sandstone containing traces of granular glauconite and organic matter. The attenuation fabric reflects the generally clean nature of the sands and there is relatively low average attenuation. Conspicuous traces of high attenuation reflect pyrite and pyritised organic matter along bedding and possibly burrow features. The sample is moderately homogeneous and no defects are evident. Although not apparent on the CT scans, traces of mercury are noted on one of the plug cut ends. Average CT Number 1281 HU, standard deviation 72 HU.

Sample Descriptions (cont'd)

Sample 30 (1774.43 m) :

An upper medium to lower coarse-grained sandstone; it contains rare flecks of organic matter. Somewhat layered concentrations of pyrite cement partially occludes pores in places. The pyrite is revealed on the CT scan as very high attenuation spots formed in poorly defined layers (e.g. py). Disseminated low attenuation spots and low average attenuation generally are evidence of open pores. However, some larger specks are inferred as organic matter (e.g. om). These organics may be pyritised (e.g. py-om). The sample is moderately homogeneous and no defects are evident. Average CT Number 1516 HU, standard deviation 260 HU.

Sample 32 1774.97 m) :

A fine-grained sandstone containing highly disturbed layers of minor siltstone and mudstone (e.g. m). The unevenly mottled attenuation fabric reflects the disturbed, probably bioturbated mix of sediments. Higher attenuation is attributable to pyrite associated with finer grain-size, particularly clays. The sample is poorly to moderately homogeneous and no defects are evident. Average CT Number 1702 HU, standard deviation 308 HU.

Sample 33 (1775.30 m) :

A very fine to fine-grained argillaceous sandstone containing highly disturbed layers of minor siltstone and mudstone (e.g. m). It has a trace of glauconite, and in places rare organic matter. The unevenly mottled attenuation fabric is similar to sample 32 and again reflects the disturbed, probably bioturbated mix of sediments. Higher attenuation is attributable to pyrite associated with finer grain-size, in particular clays. This feature is better developed in the mudstone. The sample is poorly homogeneous and no defects are evident. Average CT Number 1856 HU, standard deviation 301 HU.

Sample 34 (1775.62 m) :

A fine-grained argillaceous sandstone containing a disturbed mix of sands with variable composition as well as minor mudstone. The attenuation fabric, reminiscent of bioturbation, shows confused patches of higher attenuation. These relate to concentrations of pyrite cementing argillaceous sand (e.g. py) and pyritic mudstone (e.g. m). The sample is poorly homogeneous and no defects are evident. Average CT Number 1428 HU, standard deviation 201 HU.

APPENDIX 3
CT-SCAN AND CORE PLUG PHOTOGRAPHS

Santos Limited
Casino 2
White Light Images and Base Data

Core Lab PETROLEUM SERVICES

Santos

SAMPLE : 6
DEPTH (m): 1764.61

Ka (mD): 21.3
Por (%): 19.9
GD (g/cc): 2.66
CT No.(HU): 1610

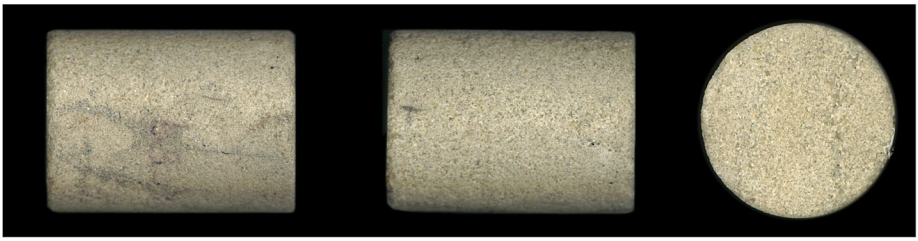

SAMPLE : 8
DEPTH (m): 1765.13

Ka (mD): 2150
Por (%): 21.5
GD (g/cc): 2.65
CT No.(HU): 1415

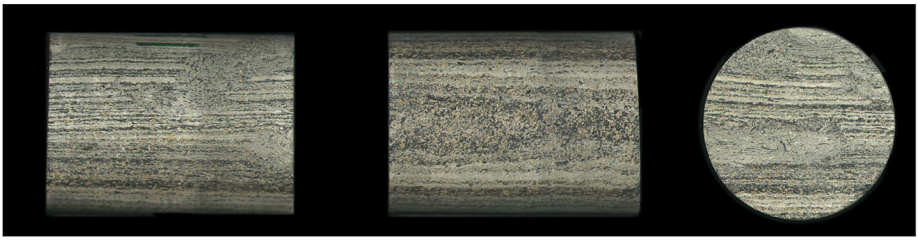

SAMPLE : 11
DEPTH (m): 1766.10

Ka (mD): 0.330
Por (%): 12.2
GD (g/cc): 2.67
CT No.(HU): 2254

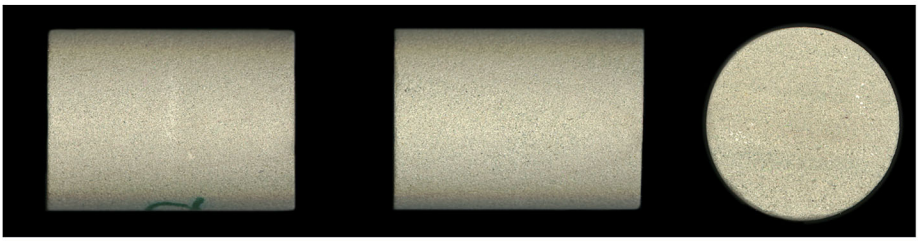

SAMPLE : 12
DEPTH (m): 1766.40

Ka (mD): *91.12
Por (%): *23.8
GD (g/cc): *2.67
CT No.(HU): 1458

* Amdel data

SAMPLE : 13
DEPTH (m): 1766.70

Ka (mD): 274
Por (%): 25.4
GD (g/cc): 2.67
CT No.(HU): 1382

SAMPLE : 14
DEPTH (m): 1767.05

Ka (mD): 0.210
Por (%): 10.2
GD (g/cc): 2.68
CT No.(HU): 1981

Coshell & Associates

Santos Limited
Casino - 2
X-ray CT Images & Base Data

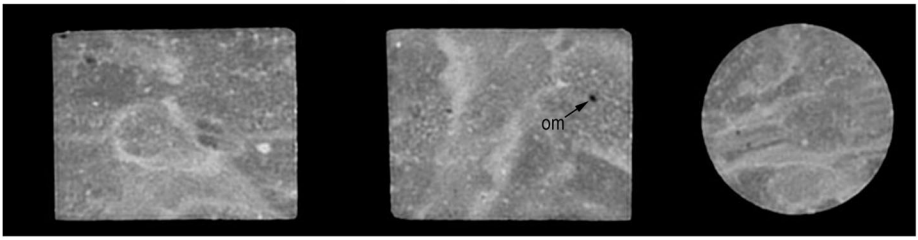

SAMPLE : 6
DEPTH (m): 1764.61

Ka (mD): 21.3
Por (%): 19.9
GD (g/cc): 2.66
CT No.(HU): 1610

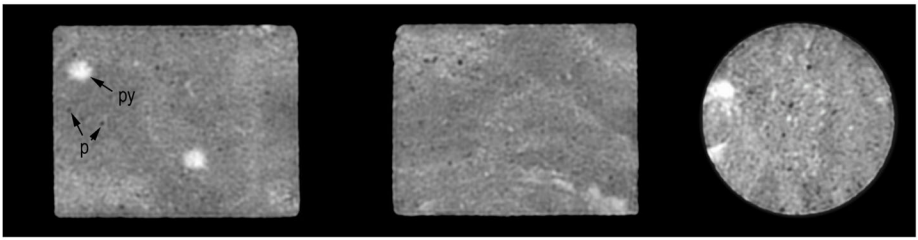

SAMPLE : 8
DEPTH (m): 1765.13

Ka (mD): 2150
Por (%): 21.5
GD (g/cc): 2.65
CT No.(HU): 1415

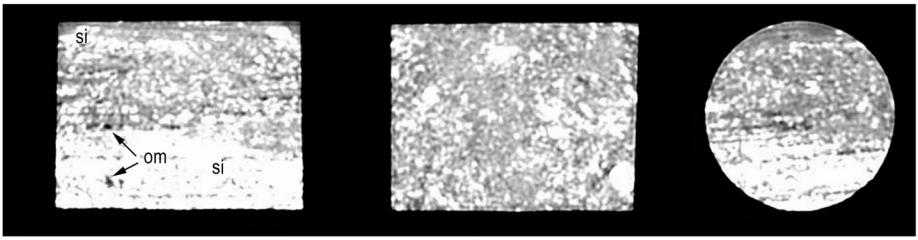

SAMPLE : 11
DEPTH (m): 1766.10

Ka (mD): 0.330
Por (%): 12.2
GD (g/cc): 2.67
CT No.(HU): 2254

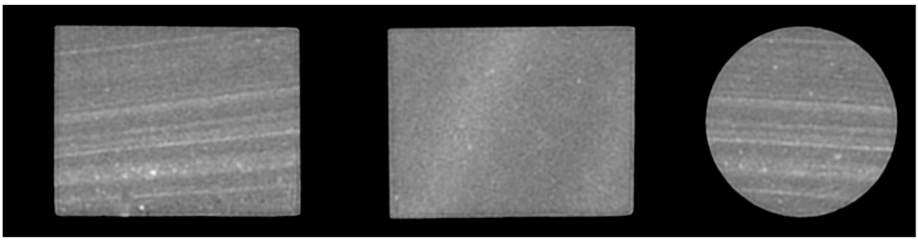

SAMPLE : 12
DEPTH (m): 1766.40

Ka (mD): *91.12
Por (%): *23.8
GD (g/cc): *2.67
CT No.(HU): 1458

* Amdel data

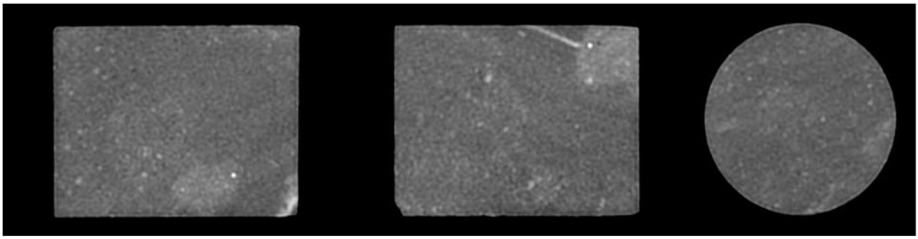

SAMPLE : 13
DEPTH (m): 1766.70

Ka (mD): 274
Por (%): 25.4
GD (g/cc): 2.67
CT No.(HU): 1382

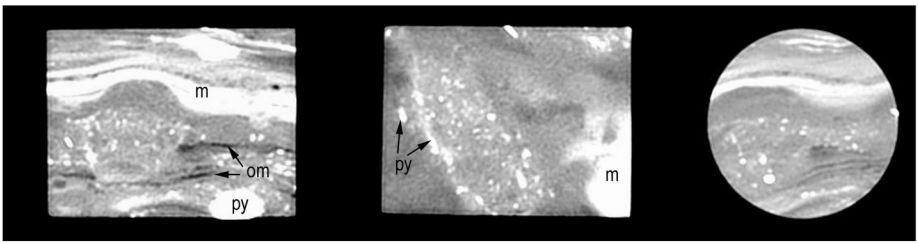

SAMPLE : 14
DEPTH (m): 1767.05

Ka (mD): 0.210
Por (%): 10.2
GD (g/cc): 2.68
CT No.(HU): 1981

Santos Limited
Casino - 2
White Light Images & Base Data

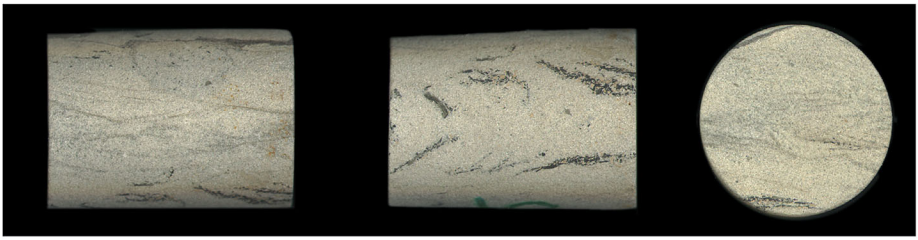

SAMPLE : 15
DEPTH (m): 1767.36

Ka (mD): 74.3
Por (%): 21.2
GD (g/cc): 2.69
CT No.(HU): 1559

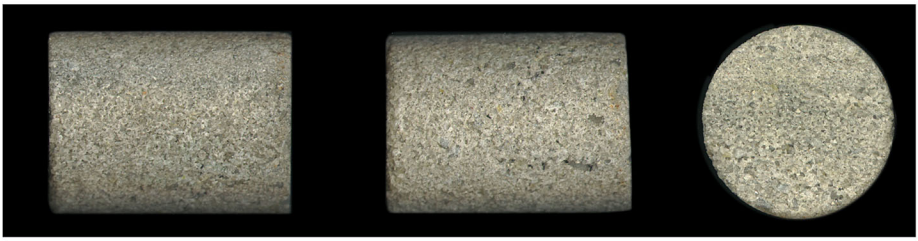

SAMPLE : 18
DEPTH (m): 1768.47

Ka (mD): *3857.16
Por (%): *19.8
GD (g/cc): *2.64
CT No.(HU): 1520

* Amdel data

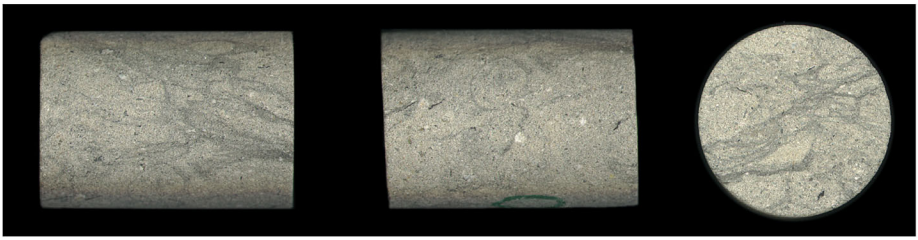

SAMPLE : 20
DEPTH (m): 1769.14

Ka (mD): 0.736
Por (%): 13.0
GD (g/cc): 2.65
CT No.(HU): 1736

SAMPLE : 21
DEPTH (m): 1769.40

Ka (mD): *3.18
Por (%): *14.1
GD (g/cc): *2.65
CT No.(HU): 1672

* Amdel data

SAMPLE : 22
DEPTH (m): 1769.70

Ka (mD): 3.84
Por (%): 15.0
GD (g/cc): 2.65
CT No.(HU): 1676

SAMPLE : 24
DEPTH (m): 1770.35

Ka (mD): 876
Por (%): 27.0
GD (g/cc): 2.66
CT No.(HU): 1281

Santos Limited
Casino - 2
X-ray CT Images & Base Data

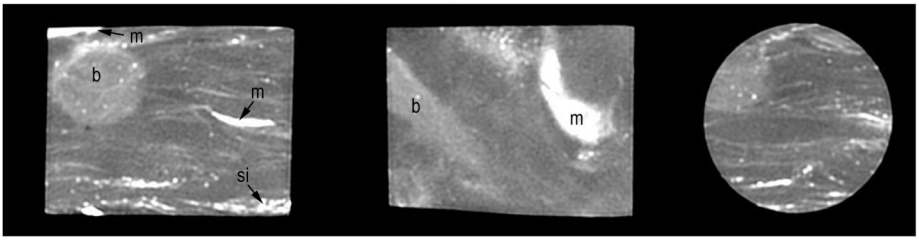

SAMPLE : 15
DEPTH (m): 1767.36

Ka (mD): 74.3
Por (%): 21.2
GD (g/cc): 2.69
CT No.(HU): 1559

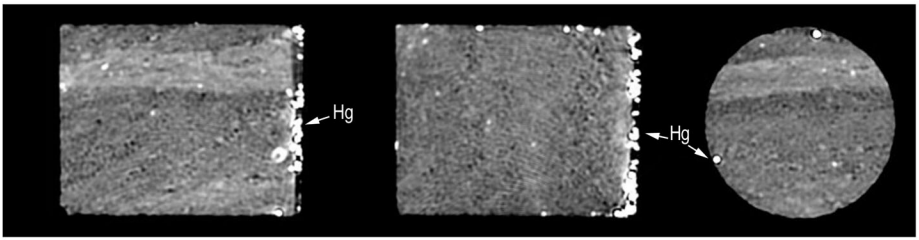

SAMPLE : 18
DEPTH (m): 1768.47

Ka (mD): *3857.16
Por (%): *19.8
GD (g/cc): *2.64
CT No.(HU): 1520

* Amdel data

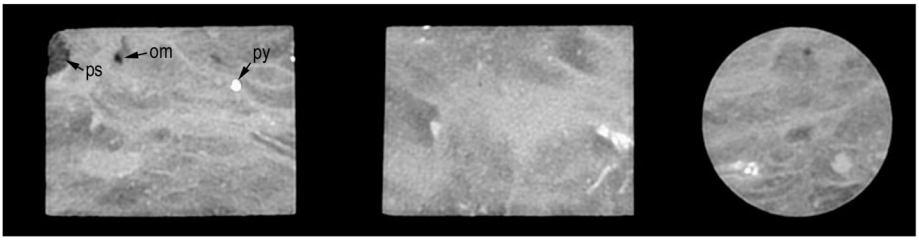

SAMPLE : 20
DEPTH (m): 1769.14

Ka (mD): 0.736
Por (%): 13.0
GD (g/cc): 2.65
CT No.(HU): 1736

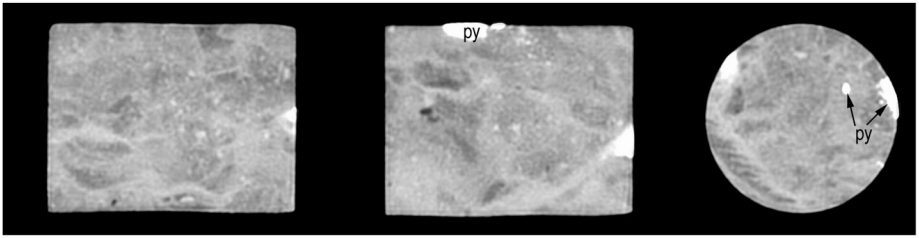

SAMPLE : 21
DEPTH (m): 1769.40

Ka (mD): *3.18
Por (%): *14.1
GD (g/cc): *2.65
CT No.(HU): 1672

* Amdel data

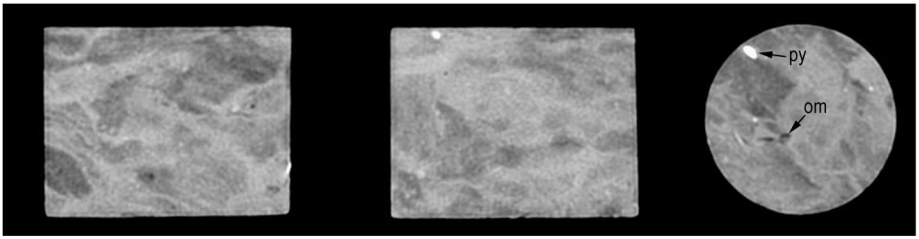

SAMPLE : 22
DEPTH (m): 1769.70

Ka (mD): 3.84
Por (%): 15.0
GD (g/cc): 2.65
CT No.(HU): 1676

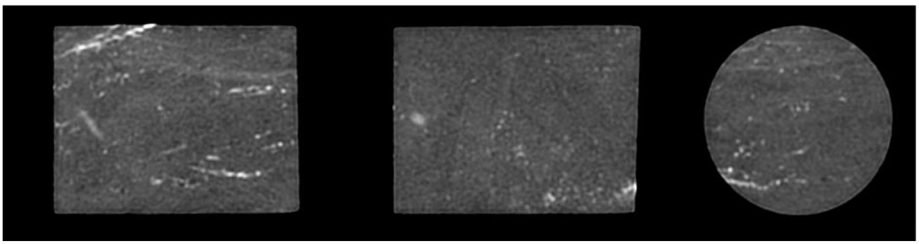

SAMPLE : 24
DEPTH (m): 1770.35

Ka (mD): 876
Por (%): 27.0
GD (g/cc): 2.66
CT No.(HU): 1281

Coshell & Associates

Santos Limited
Casino - 2
White Light Images & Base Data

SAMPLE : 30
DEPTH (m): 1774.43

Ka (mD): 3650
Por (%): 20.8
GD (g/cc): 2.69
CT No.(HU): 1516

SAMPLE : 32
DEPTH (m): 1774.97

Ka (mD): *69.18
Por (%): *19.4
GD (g/cc): *2.72
CT No.(HU): 1702

* Amdel data

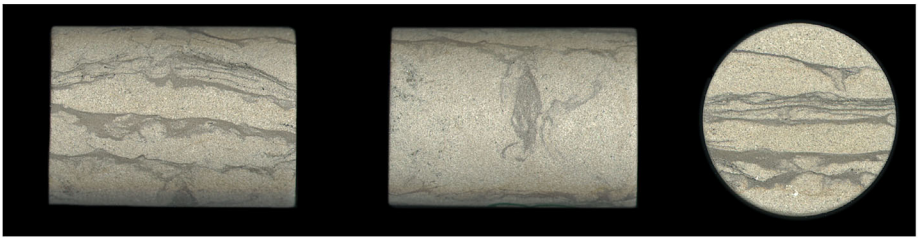

SAMPLE : 33
DEPTH (m): 1775.30

Ka (mD): 13.4
Por (%): 17.6
GD (g/cc): 2.68
CT No.(HU): 1856

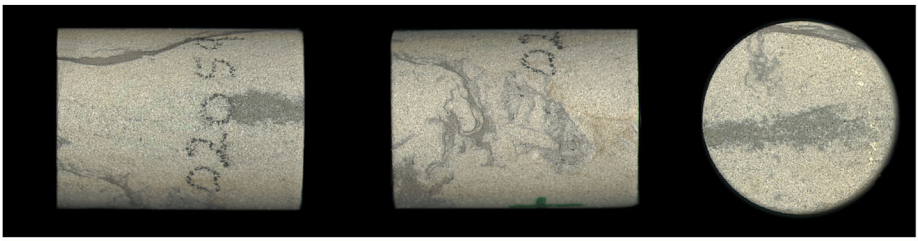

SAMPLE : 34
DEPTH (m): 1775.62

Ka (mD): 232
Por (%): 23.2
GD (g/cc): 2.70
CT No.(HU): 1428

Santos Limited
Casino - 2
X-ray CT Images & Base Data

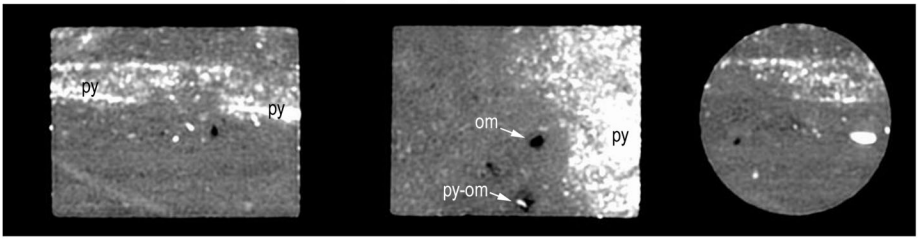

SAMPLE : 30
DEPTH (m): 1774.43

Ka (mD): 3650
Por (%): 20.8
GD (g/cc): 2.69
CT No.(HU): 1516

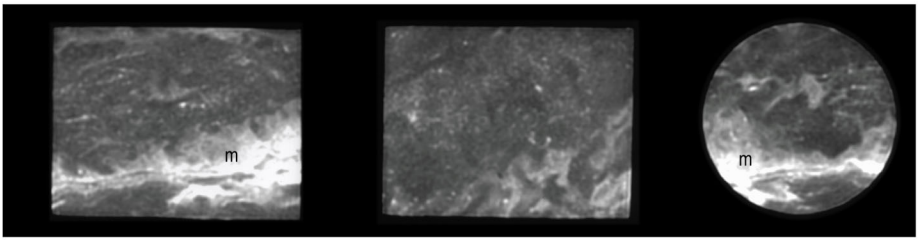

SAMPLE : 32
DEPTH (m): 1774.97

Ka (mD): *69.18
Por (%): *19.4
GD (g/cc): *2.72
CT No.(HU): 1702

* Amdel data

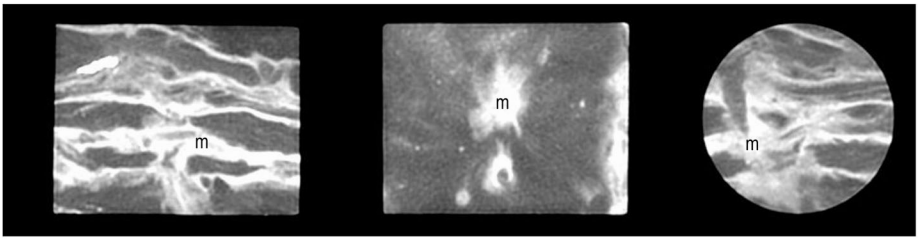

SAMPLE : 33
DEPTH (m): 1775.30

Ka (mD): 13.4
Por (%): 17.6
GD (g/cc): 2.68
CT No.(HU): 1856

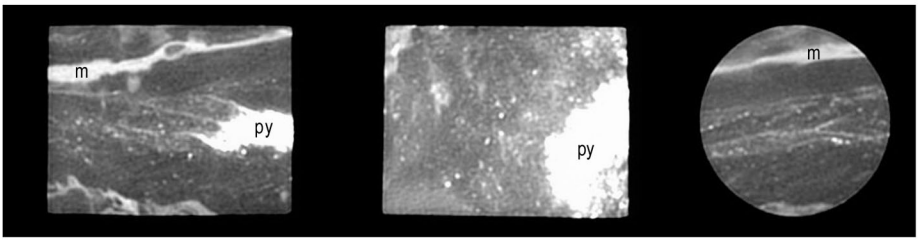

SAMPLE : 34
DEPTH (m): 1775.62

Ka (mD): 232
Por (%): 23.2
GD (g/cc): 2.70
CT No.(HU): 1428